Effect of excitons in quantum spin Hall effect

Author:
Tania Paul

Supervisors:
Dr. Timo Hyart
Dr. hab. Wojciech Brzezicki

Submitted in partial fulfillment of the requirements for the degree of

DOCTOR OF PHILOSOPHY

August 21, 2023

INTERNATIONAL RESEARCH CENTER MAGTOP,
INSTITUTE OF PHYSICS, POLISH ACADEMY OF SCIENCES, WARSAW, POLAND

To my parents

"*We spent our day looking under rocks in the creek...*"

- Bill Watterson, *Calvin and Hobbes,* 30 June 1992

Acknowledgement

I would like to begin by conveying my gratitude to Timo, without whom the completion of the two research projects that comprise this thesis would not have been possible. Apart from being an excellent physicist, he has also been a wonderful PhD guide right from the beginning. He created a positive and collaborative work environment, where I was given the time to learn from my failures and improve my research capabilities. His dedication and approach to research is inspiring and made working with him rewarding.

I would like to give my sincere thanks to Victor, who has consistently made time to help me when I was stuck with computational or analytical problems. I have also learnt a lot from his exceptional coding skills and his approach to work. During his time at the institute, he always gave me space to discuss and cleared my conceptual doubts with respect to our research.

I would like to thank Dr. hab. Wojciech Brzezicki for his support and help with the thesis. I am thankful to Prof. Tomasz Dietl and Prof. Tomasz Wojtowicz for their numerous help during this period. I would also like to extend my thanks to Dr. hab. Carmine Autieri, for letting me use his computational grant in my first year and providing me with important information regarding the doctoral procedures at the institute.

Even though we were not research collaborators, Archana has listened to my silly physics questions every time. The discussions and laughter we shared in the office translated to a genuine friendship which I will always cherish. I would like to thank Nguyen, who was my first friend in the institute and with whom I have also shared many laughs and discussions. Ashutosh, who has inspired me with his contagious enthusiasm for physics and design ideas. To Arathi, Saranya, Sarath, Giuseppe and Peixin for joys of friendship. To Anna, Agnieszka, Sylwia and Bozena for their assistance during this period.

To Lekha ma'am for believing in me and pushing me to do better. To Tabish sir for introducing me to theoretical research. Lastly, I am grateful and indebted to my parents for always encouraging my dreams and life decisions, my husband Umair for

his love and support, and my folks from back home.

Abstract

A quantum spin Hall insulator is a two-dimensional insulator with an insulating bulk and conducting edges. They belong to an entirely new class of materials which cannot be adiabatically connected to usual (topologically trivial) insulators and semiconductors. Much like the quantum Hall and quantum anomalous Hall effects, the quantum spin Hall effect also finds connection to topology to explain its many interesting features. After establishing key concepts related to topological materials in general and quantum spin Hall effect in particular, this thesis begins an investigation into electron-hole correlations in the quantum spin Hall effect of band-inverted electron-hole bilayers. The Coulomb interactions favors the formation of excitons, a pair of electron and hole from the conduction and valence bands, respectively, that condense to form a highly coherent phase. Excitonic correlations enrich the topological phase diagram of quantum spin Hall insulators by inducing an insulating phase with spontaneously broken time-reversal symmetry between the trivial and quantum spin Hall phases. One of the paradigmatic features of topological phase transitions in correlation-free topological insulators is the bulk-gap closing. However, the presence of excitons lead to a transition where the bulk-gap does not close. This could be interpreted as an effort by the system to minimise energy during the topological transition. There are multiple, recent experimental observations pointing out the existence of excitons in these systems but so far the spontaneous time-reversal symmetry breaking has not been directly observed. In the original work carried out for this thesis, we propose an experimental set-up to observe this time-reversal symmetry broken phase. Numerical experiments of transport in a Corbino disc measure bulk and edge conductances and confirm that the topological phase transition manifests without bulk-gap closing. Moreover, we also propose to utilize the system in its broken time-reversal symmetry state, together with an s-wave superconductor, to create, probe and manipulate the appearance of Majorana zero modes. We find, both numerically and analytically, the existence of Majorana zero modes at the interface of an s-wave superconductor and a time-reversal symmetry broken insulator. We provide an experimental configuration of a superconductor/TRS broken insulator/superconductor Josephson junction to observe 4π Josephson current, which is indicative of the Majorana zero modes residing at the interface. Finally, we also propose how to manipulate the quantum information stored in the Majorana zero modes and read out the state of the topological qubit.

Streszczenie

Kwantowe spinowe izolatory Halla to układy dwuwymiarowe z izolującą objętością i przewodzącymi krawędziami. Należą one do zupełnie nowej klasy materiałów, których nie da się połączyć adiabatycznie ze zwykłymi (topologicznie trywialnymi) izolatorami i półprzewodnikami. Podobnie jak kwantowy i kwantowy anomalny efekt Halla, kwantowy spinowy efekt Halla również wiąże się z topologią, co pozwala wyjaśnić jego wiele interesujących cech. Po ustaleniu kluczowych pojęć związanych ogólnie z materiałami topologicznymi, a w szczególności z kwantowym spinowym efektem Halla, niniejsza praca skupia się na badaniu korelacji elektron-dziura w układach dwuwarstwowych z odwróconymi pasmami. Oddziaływania kulombowskie sprzyjają tworzeniu ekscytonów, par elektronów i dziur odpowiednio z pasm przewodnictwa i walencyjnego, które kondensują, tworząc wysoce koherentną fazę. Korelacje ekscytonowe wzbogacają topologiczny diagram fazowy kwantowych spinowych izolatorów Halla, indukując fazę izolującą ze spontanicznie złamaną symetrią odwrócenia czasu, pomiędzy trywialną i nietrywialną fazą spinowego izolatora Halla. Jedną z charakterystycznych cech topologicznych przejść fazowych w bezkorelacyjnych izolatorach topologicznych jest zamykanie przerwy energetycznej. Obecność ekscytonów prowadzi jednakże do przejścia, w którym przerwa nie zamyka się. Można to interpretować jako wysiłek systemu w celu zminimalizowania energii podczas przejścia topologicznego. Istnieje wiele niedawnych obserwacji doświadczalnych wskazujących na istnienie ekscytonów w układach dwuwarstwowych, ale jak dotąd nie zaobserwowano bezpośrednio spontanicznego łamania symetrii odwrócenia czasu. W oryginalnych badaniach przeprowadzonych na potrzeby tej rozprawy proponujemy układ doświadczalny do obserwacji tej właśnie fazy uporządkowanej. Numeryczne obliczenia transportu w dysku Corbino, badające przewodnictwo w objętości i na krawędziach, potwierdzają, że topologiczne przejście fazowe odbywa się bez zamykania przerwy energetycznej. Co więcej, proponujemy również wykorzystanie układu w jego stanie ze złamaną symetrią, wraz z nadprzewodnikiem typu s, do tworzenia, badania i manipulowania stanami zerowymi Majorany. Potwierdzamy, zarówno numerycznie jak i analitycznie, istnienie stanów zerowych Majorany na gra-

nicy tych dwóch układów. Przedstawiamy eksperymentalną konfigurację złącza Josephsona o budowie: nadprzewodnik/izolator ze złamaną symetrią/nadprzewodnik, pozwalającą zaobserwować prąd Josephsona o okresie 4π, wskazujący na stanami zerowymi Majorany zlokalizowane na interfejsach. Na koniec pokazujemy również, jak manipulować informacją kwantową przechowywaną w stanach zerowych Majorany i odczytywać stan kubitu topologicznego.

List of publications

1. **T. Paul**, V. Fernández Becerra, T. Hyart, Interplay of quantum spin Hall effect and spontaneous time-reversal symmetry breaking in electron-hole bilayers. I. Transport properties, Phys. Rev. B 106, 235420 (2022).
2. **T. Paul**, V. Fernández Becerra, T. Hyart, Interplay of quantum spin Hall effect and spontaneous time-reversal symmetry breaking in electron-hole bilayers. II. Zero-field topological superconductivity, Phys. Rev. B 106, 235421 (2022).

List of oral presentations

1. **T. Paul**, V. Fernández Becerra, T. Hyart, Effect of excitons in type-II quantum wells, International meeting on superconducting quantum materials and nanodevices, April 2023, Budva, Montenegro (**Invited talk**).
2. **T. Paul**, V. Fernández Becerra, T. Hyart, Interplay of excitonic correlations,quantum spin Hall effect and superconductivity in electron-hole bilayers, Joint European Magnetic Symposia, July 2022, Warsaw, Poland (**Contributed talk**).
3. **T. Paul**, V. Fernández Becerra, T. Hyart, Interplay of excitonic correlations with quantum spin Hall effect and superconductivity, 3rd annual conference Q-MAT 2020, Kolkata, India (**Online talk**)

Contents

1 Introduction **4**

1.1 Quantum Hall effect 6

1.1.1 Edge states 8

1.1.2 Topological explanation of the perfect quantization of Hall resistance 8

1.1.3 Other remarks 10

1.2 Quantum anomalous Hall effect 11

1.2.1 Haldane model in honeycomb lattices 11

1.2.2 Qi-Wu-Zhang model 13

1.3 The quantum spin Hall effect 16

1.3.1 Inverted band structure 18

1.3.2 Time reversal symmetry 19

1.3.3 $\mathbb{Z}_2$ Topological invariant 19

1.3.4 Quantized conductance 20

1.3.5 Experimental signatures 21

1.4 Role of interactions 22

1.5 Majorana zero modes 23

1.6 Quantum transport theory 27

1.7 Motivation and outline 29

1.7.1 Motivation 29

1.7.2 Outline 31

2 Bernevig-Hughes-Zhang model for the quantum spin Hall effect **33**

2.1 Quantum well structure 34
2.1.1 Type-I quantum well 34
2.1.2 Type-II quantum well 35
2.2 Non-interacting BHZ model 36
2.3 Symmetries of the system 37
2.3.1 Inversion symmetry 37
2.3.2 Rotation symmetry 38
2.3.3 Time-reversal symmetry 38
2.4 Model parameters 38
2.5 Effect of bulk inversion asymmetry Δ_z term 39
2.5.1 Type-I quantum well 39
2.5.2 Type-II quantum well 41
2.6 Effect of mass asymmetry 41
2.7 Topological Invariant 42
2.7.1 Spin Chern topological invariant when $\Delta_z = 0$ 43
2.7.2 Z_2 topological invariant when $\Delta_z \neq 0$ 45
2.8 Effect of magnetic field 49
2.8.1 Perpendicular magnetic field 49
2.8.2 In-plane magnetic field 50

3 Interplay of excitons and the quantum spin Hall effect 52
3.1 Excitons in Type-II quantum well 52
3.1.1 Obtaining the exciton pairings 54
3.2 Topological Phase transition 56
3.3 Bulk inversion asymmetry term Δ_z 60
3.4 Mass asymmetry 61

4 Paper I: Interplay of quantum spin Hall effect and spontaneous time-reversal symmetry breaking in electron-hole bilayers I. Transport properties 63

5 Paper II: Interplay of quantum spin Hall effect and spontaneous time-reversal symmetry breaking in electron-hole bilayers II. Zero-field Topological Superconductivity 75

6 Conclusion and Outlook 94

Bibliography 95

List of Figures

1.1 Hall resistance as a function of magnetic field 5
1.2 Quantum Hall effect 7
1.3 Quantum Hall effect without Landau levels 13
1.4 Qi-Wu-Zhang model 15
1.5 Quantum spin Hall effect in graphene 17
1.6 Quantized conductance for Bernevig, Hughes and Zhang model . . . 20
1.7 Two-terminal setup to measure edge conductance 21
1.8 Kitaev's chain 25
1.9 Experimental setups to observe Majorana zero modes 26
1.10 Quantum transport setup 27

2.1 Type-I quantum well structure and bulk band structure 35
2.2 Type-II quantum well structure and bulk band structure 36
2.3 Edge spectrum of a type-I quantum well when $\Delta_z = 0$ 40
2.4 Edge spectrum of a type-I quantum well when $\Delta_z \neq 0$ 40
2.5 Edge spectrum of a type-II quantum well when $\Delta_z \neq 0$ 41
2.6 Edge spectrum with mass asymmetry between electrons and holes . . 42
2.7 Spin Chern number as a function of E_G 45
2.8 The zeros of $P(k)$ lying on a curve enclosing the Γ point, when the system is in quantum spin Hall phase. 48

3.1 Phase diagrams of $\Delta_{1,2}$ for different g_s and g_p 55
3.2 Phase diagram of $\mathcal{T}_{br}$ 57
3.3 Phase diagram of $\mathcal{P}$ 58

3.4 Energy band dispersion 59
3.5 Phase diagram of order parameters for different Δ_z 60
3.6 Phase diagram for mass asymmetry 61
3.7 Energy phase diagram in the presence of mass asymmetry 62

List of Tables

2.1 Table of parameter values used for the calculations present in this thesis for HgTe/CdTe and InAs/GaSb. Table adapted from [133]. . . 39

Chapter 1

Introduction

In 1879, Edwin Hall showed that, a perpendicular magnetic field applied to a thin metallic sheet, can induce an electric voltage perpendicular to the charge current [1]. Hall effect is now an important technique used to charecterize semiconducting films to obtain the carrier density n_s and mobility μ through the measurement of Hall resistance ρ_{xy} and longitudinal resistance ρ_{xx},

$$\rho_{xy} = \frac{B}{en_s}, \qquad \text{and} \qquad \rho_{xx} = 1/en_s\mu, \tag{1.1}$$

where e is the magnitude of the electronic charge and B is the magnetic field applied perpendicularly [2]. In 1980, it was experimentally shown that, a two-dimensional electron gas in the inversion layer of a silicon based MOSFET (metal-oxide semiconductor field-effect transistor) exposed to a strong magnetic field (> 18 T) at low temperatures gives rise to quantized steps of Hall resistance [3]. It was also accompanied by an oscillating longitudinal resistance. The longitudinal resistance were finite-valued peaks at the transition between two Hall resistance plateaus and zero otherwise (see Fig. 1.1). This behaviour is in contrast to (1.1), where the Hall resistance is linearly proportional to B and the longitudinal resistance is a constant.
Implementing the theory of Landau quantization, gave some understanding of the new observations [2]. The quantization of Hall resistance was explained as the num-

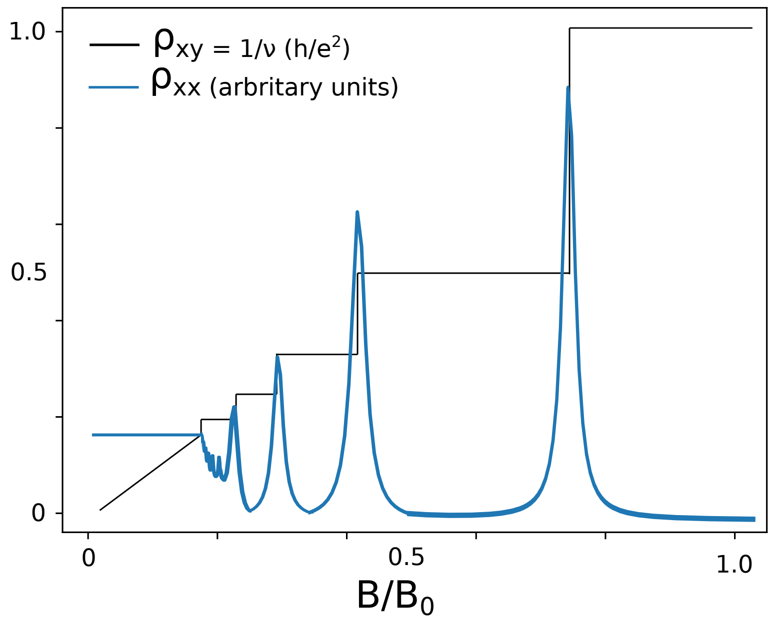

Figure 1.1: Schematic illustration of Hall resistance ρ_{xy} and longitudinal resistance ρ_{xx} as a function of B/B_0, where $B_0 = n_s h/e$, applied perpendicularly to a two-dimensional electron gas. The Hall resistance forms quantized plateaus of values $1/\nu$ (is linear) as a function of strong (weak) applied magnetic field B/B_0. The longitudinal resistance shows oscillatory (constant) behaviour for strong (weak) magnetic field.

ber of filled Landau levels and was given by

$$\rho_{xy} = \frac{1}{\nu}\frac{h}{e^2} \implies \sigma_{xy} = \frac{e^2\nu}{h}, \tag{1.2}$$

where the integer $\nu = 1, 2, 3...$. The longitudinal resistance is zero when the Hall resistance is quantized and when the integer value of ν changes, the longitudinal resistance shows finite height peaks (see Fig. 1.1). When the Fermi energy lies in between two Landau levels, the Hall resistance takes a quantized value and longitudinal resistance becomes zero. When the Fermi energy lies on a Landau level, the quantization breaks and the longitudinal resistance ceases to be zero and takes a finite value. Presence of disorder with strength smaller than the energy gap between the Landau levels, were considered essential to explain the plateau formation in Hall resistance [4, 5].

This experiment was repeated for different materials [6, 7], and the observation of a perfectly quantized Hall resistance was found to be consistent in all these experiments. The observation of the quantum Hall effect is often considered to be one of the most significant discoveries in twentieth century physics, and von Klitzing was awarded the Nobel prize in physics in 1985 [8]. The quantum Hall effect laid a foundation for the observation of even more intricate physics like fractional quantum Hall effect [9–11], exciton condensation [12], the quantum spin Hall effect [13, 14] and quantum anomalous effect [15–17]. It has also opened up research to find non-Abelian quasiparticles that could be used in topological quantum computation [18]. The quantum Hall effect has analogies even in the study of black holes and string theory [19, 20].

Below, we will discuss the physics behind quantum Hall effect and quantum anomalous Hall effect to better understand the quantum spin Hall effect. The former two theories are crucial in understanding the topological nature of quantum spin Hall effect. We will then look into the important properties of quantum spin Hall effect, role of interactions in quantum spin Hall insulators, and its application in realizing Majorana zero modes which are useful in topological quantum processing. A short section on quantum transport theory is also included, as the method is used to calculate the bulk and edge conductance in the paper attached in Chapter 4. This will be followed by presenting the main research problems addressed in the thesis and the thesis outline.

1.1 Quantum Hall effect

The theory of Landau quantization of energy states [2, 21, 22] was used initially to get the expression for the quantized Hall conductance given in (1.2). However, what surprised the scientific community the most was the order of accuracy ($\sim 10^{-9}$) of the Hall conductance [6, 23]. Why is a disordered sample in a quantum Hall setup producing a quantized current of such high accuracy? Moreover, Laughlin in 1981 introduced gauge invariance to explain the quantized Hall resistance [4]. He considers a flux Φ that introduces a gauge potential going through the center of a Corbino ring in addition to the magnetic field. To see this roughly, consider that flux Φ is slowly changing from zero to $\Phi_0 = 2\pi\hbar/e$ over the time 0 to T. An electro-

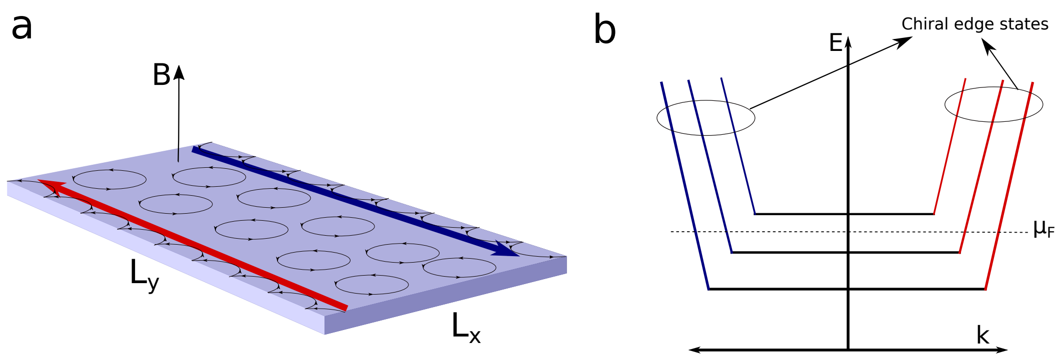

Figure 1.2: (a) Schematic figure depicting quantum Hall effect. The chiral edge states are shown by red and blue arrows. The classical picture of cyclotron orbits and skipping orbits at the edge is also depicted. Since the spin of the electron does not enter the equation of motion, both spin-up and spin down electrons will show the same behaviour in motion as shown in the figure. Figure adapted from [25]. (b) Schematic illustration of the energy states giving rise to the chiral edge states. Figure adapted from [2].

motive force $\mathcal{E} = -\partial\Phi/\partial t = -\Phi_0/T$ appears around the ring. If a fixed n number of electrons are transported from the inner edge of the ring to the outer edge of the ring, then the radial current $I = -en/T$, and the Hall resistance comes out to be

$$\rho_{xy} = \frac{\mathcal{E}}{I} = \frac{\Phi_0}{ne} = \frac{h}{e^2}\frac{1}{n}. \tag{1.3}$$

The above thought experiment is called *Laughlin's charge pumping* and it was experimentally proven recently using an ultracold atomic gas [24]. When n number of electrons are transferred from the inner edge to the outer edge of the ring, the bulk is considered to be gapped and longitudinal resistance is zero. Of course, this explanation is true only in the case of integer quantum Hall effect as the quasiparticles that are transferred carries electron charge. In the case of fractional quantum Hall effect, the transferred quasiparticles carry fractional charge. While Lauglin's charge pumping argument does not directly apply to the experimental setup of quantum Hall effect, it alluded to the presence of something deeper and more fundamental to the theory of quantum Hall effect [22]. Below, we will see how a combination of different approaches is required to attain clarity regarding quantum Hall effect.

1.1.1 Edge states

One of the interesting observations from the study of quantum Hall systems is the presence of robust, unidirectional states that move along the boundary of the material. Consider a rectangular sample which is finite in, say, x direction and is infinite in the y direction. A magnetic field B is applied perpendicular to the plane of this sample. Classically, one can see electrons make incomplete cyclotron orbits or skipping orbits at the boundary of the sample as shown in Fig. 1.2a. These skipping orbits move in opposite directions on boundaries opposite to each other. From quantum mechanics, the edge modes are explained by the presence of a confining potential. For a wide sample, along the x direction, the confining potential can look very flat in the bulk, with steep rise (fall) on the right (left) edge. This leads the electrons to move in opposite directions on the right and left edges. For a wide enough sample along the x direction, the two edge states are spatially separated and will have little overlap. Therefore, any impurity on one edge cannot scatter the electron to the opposite edge, making these edge states very robust. These unidirectional edge states are called *chiral edge states*. In the bulk, the electrons have zero drift velocity because of the very flat confining potential in the interior of the sample.

Within the edge state picture, the quantization of Hall resistance and zero longitudinal resistance is explained using the Landauer-Buttiker formalism (see Chapter 2 and 4 in Ref. [2]). The quantized Hall resistance is shown to be dependent on the number of edge states at the Fermi energy which in turn, is equal to the number of filled Landau levels. The bulk states that contribute to longitudinal resistance remain in equilibrium and hence do not contribute to transport [2].

1.1.2 Topological explanation of the perfect quantization of Hall resistance

Laughlin's charge pumping thought experiment and the edge state explanation of the quantized Hall conductance were followed by a work by Thouless-Kohomoto-Nightingale-den Nijs in 1982 where the quantized Hall conductance is related to a topological invariant in two-dimensional systems [26]. In this case the quantized Hall conductance is obtained from the bulk-current density when an electric field is applied.

Consider a particle moving in a rectangular lattice, where the lattice momentum is restricted to the Brillouin zone of the reciprocal lattice [27, 28]. This Brillouin zone can also be described by a torus $\mathbf{T}^2$ that is parameterised by k_x and k_y. Moreover, there is no electron-electron interaction present and the Fermi energy lies between the filled and unfilled bands. With these assumptions, using the Kubo formula, when an electric field E_x is applied in the x direction, the bulk current density j_y obtained will yield the Hall conductivity, given by,

$$\sigma_{xy} = \frac{ie^2}{\hbar} \sum_{\alpha} \int_{\mathbf{T}^2} \frac{d^2k}{(2\pi)^2} \left\langle \partial_y u_{\mathbf{k}}^{\alpha} | \partial_x u_{\mathbf{k}}^{\alpha} \right\rangle - \left\langle \partial_x u_{\mathbf{k}}^{\alpha} | \partial_y u_{\mathbf{k}}^{\alpha} \right\rangle . \tag{1.4}$$

Here, the sum is over occupied energy bands α, ∂_i is a shorthand-notation for $\partial/\partial k_i$, and $|u_{\mathbf{k}}^{\alpha}\rangle$ is an eigenstate of the Hamiltonian corresponding to band α that picks up a phase as it completes a round in the Brillouin zone [22, 29]. The integrand can be obtained using the expressions for the Berry connection and Berry curvature [30–32]. The Berry connection measures the change in gauge and is given by

$$\mathcal{A}_i(\mathbf{k}) = -i \left\langle u_{\mathbf{k}} \right| \frac{\partial}{\partial k^i} \left| u_{\mathbf{k}} \right\rangle , \tag{1.5}$$

where $i = x, y$. The Berry curvature is defined as the curl of the Berry connection,

$$\Omega_{xy} = \frac{\partial \mathcal{A}_x}{\partial k^y} - \frac{\partial \mathcal{A}_y}{\partial k^x} = -i \left\langle \partial_y u | \partial_x u \right\rangle + i \left\langle \partial_x u | \partial_y u \right\rangle . \tag{1.6}$$

Integration of the Berry curvature over the Brillouin zone gives us the Chern number,

$$C = -\frac{1}{2\pi} \int_{\mathbf{T}^2} \Omega_{xy}. \tag{1.7}$$

When the Chern number for each filled band α is calculated and summed over, the Hall conductance which is observed in the experiments is obtained,

$$\sigma_{xy} = \frac{e^2}{2\pi\hbar} \sum_{\alpha} C_\alpha. \tag{1.8}$$

The summation of Chern number over all the filled bands is an integer which is termed as TKNN number and gives the value for Hall conductance. It is a topological invariant which does not change as long as the energy gap does not close [26]. Interestingly, this theory tells us that measuring Hall resistance indicates the topological state of a system. In the quantum Hall effect, the Chern number is a nonzero integer that comes from the structure of the wave functions of the Landau levels that are formed in the presence of a strong magnetic field. These equations show why the Hall resistance is an integer number that is not dependent on any details of material properties, but on a topological invariant called the Chern number. This connection between Hall conductivity and a topological invariant naturally provides an explanation why robust quantization is observed for Hall resistance. Moreover, between each Hall resistance plateau, the bulk-gap closes and leads to a peak in the longitudinal resistance as well as a change in Chern number.

1.1.3 Other remarks

We have presented two pictures to understand the quantized Hall conductance. The edge state picture suggests that the current is carried only by the chiral edge states at the Fermi energy, whereas the TKNN picture shows that the bulk states also participate in the quantized Hall conductance. There are also other works which give different descriptions of the spatial distribution of the current that flows in the bulk [6, 33] and along the edge [34]. By keeping the microscopic details aside, the edge state and TKNN pictures are nicely connected via *bulk-boundary correspondence*. The bulk-boundary correspondence ensures that the Chern number is equal to the number of *chiral edge states*. As long as the bulk-gap does not close, the Chern number will not change. Therefore, the edge states remain topologically protected through the bulk [35–38], and the spatial distribution of the current does not affect the quantization of the Hall conductance.

The quantization of Hall conductance occurs at precise integers in units of e^2/h . Hence it is also called the *integer quantum Hall effect*. There also exists a *fractional quantum Hall effect*, where the quantization of Hall conductance occurs at extremely accurate fractional values due to the presence of strongly-interacting electrons [9, 11]. Robert B. Laughlin, Horst L. Störmer and Daniel C. Tsui shared a Nobel prize in 1998 for the discovery of fractional quantum Hall effect [39]. There continues to be new developments and revisions to the theory of quantum Hall effect [40, 41]. The quantum Hall effect can also be realized in three-dimensional systems, but the physics behind this effect differs from that for the two-dimensional systems [42–44]. It has also been demonstrated that the quantum Hall effect in graphene and other Dirac fermion systems can be realized at significantly higher temperatures because the energy gaps between the Landau levels are larger at a given magnetic field [45].

1.2 Quantum anomalous Hall effect

The observation of quantized Hall conductance in two dimensional electron gas without an external magnetic field is referred to as quantum anomalous Hall effect [46–48]. The materials exhibiting quantum anomalous Hall effect are also called Chern insulators because the topological invariant in these systems, is the Chern number which was discussed above.

1.2.1 Haldane model in honeycomb lattices

In 1988, F.D.M Haldane put forward a theoretical proposal to observe the quantized Hall conductance in systems with a honeycomb lattice structure, like graphene, when no net magnetic field is applied perpendicularly [15]. Hobeycomb lattices have both inversion and time-reversal symmetry which leads to the valence and conduction band to meet at two corners K and K' of the Brillouin zone. Breaking one of the two symmetries will produce a gap at $K(K')$. In Haldane's proposal, it is argued that there exist a suitable symmetry-breaking perturbation so that when the Fermi energy lies in the center of this gap, a quantized Hall conductance is obtained just as discussed above.

In the model, a next-nearest neighbor (NNN) hopping t_2 is introduced in addition to the nearest neighbor (NN) t_1 term. Moreover, the model includes a local magnetic flux density perpendicular to the unit cell such that the total flux through the unit cell remains zero. Due to this local field, the electron picks up a phase ϕ when it goes to its next-nearest neighbor (see Fig.1.3a). The tight-binding Hamiltonian for this model becomes,

$$\begin{aligned} H(\mathbf{k}) &= 2t_2 \cos\phi \left(\sum_i \cos(\mathbf{k} \cdot b_i) \right) \sigma_0 + t_1 \left(\sum_i [\cos(\mathbf{k} \cdot a_i)\sigma_x + \sin(\mathbf{k} \cdot a_i)\sigma_y] \right) \\ &\quad + \left[M - 2t_2 \sin\phi \left(\sum_i \sin(\mathbf{k} \cdot b_i) \right) \right] \sigma_z, \end{aligned} \tag{1.9}$$

where σ's are the Pauli matrices, M is the difference in onsite energies of the two different sublattices A and B, and a_i and b_i are the lattice vectors between NN and NNN points. If $t_2, M << t_1$, then the above tight-binding Hamiltonian can be expanded around K and K' as

$$H_{\mathbf{K}(\mathbf{K}')} = \mp \frac{3t_1}{2}(k_x\sigma_x \pm k_y\sigma_y) + m_\pm \sigma_z, \tag{1.10}$$

which describes the (2+1)D Dirac Hamiltonian where, $m_\pm = M \pm 3\sqrt{3}t_2 \sin\phi$ behaves like the Dirac mass term. If $m_\pm \neq 0$ it induces an energy gap around K and K'. $M \neq 0$ breaks the inversion symmetry while $t_2 \sin\phi \neq 0$ breaks time-reversal symmetry. If t_2 is positive valued, then varying M term from negative to positive values can change the sign of the Dirac mass term. A particular value of M will cancel the $t_2 \sin\phi$ term, and the Dirac mass term will become zero. The sign of this mass term determines the value of the Hall conductivity through the relation $\sigma_{xy} = Ce^2/h$, where

$$C = \frac{1}{2}[\text{sgn}(m_-) - \text{sgn}(m_+)]. \tag{1.11}$$

When $t_2 \sin\phi = 0$, then $\mathrm{sgn}(m_-) = \mathrm{sgn}(m_+)$ and the time-reversal symmetry is preserved. This gapped system is adiabatically connected to a normal semiconductor which does not exhibit quantized Hall conductance. When both $M \neq 0$ and $t_2 \sin\phi \neq 0$, their signs and relative strengths determine the value of $C = \pm 1, 0$. When $C = 0$, then m_- and m_+ have the same sign or time-reversal symmetry is not broken. C is the Chern number determining the quantized Hall conductance. The three phases with zero Chern number and non-zero Chern number are all separated by bulk-gap closings. The bulk-gap closing forms the phase boundaries in the topological phase diagram shown in Fig.1.3b. The experimental confirmation of this model has so far been unsuccessful in stand alone two-dimensional materials with honeycomb lattice but have been shown using ultracold atoms in an optical honeycomb lattice [49].

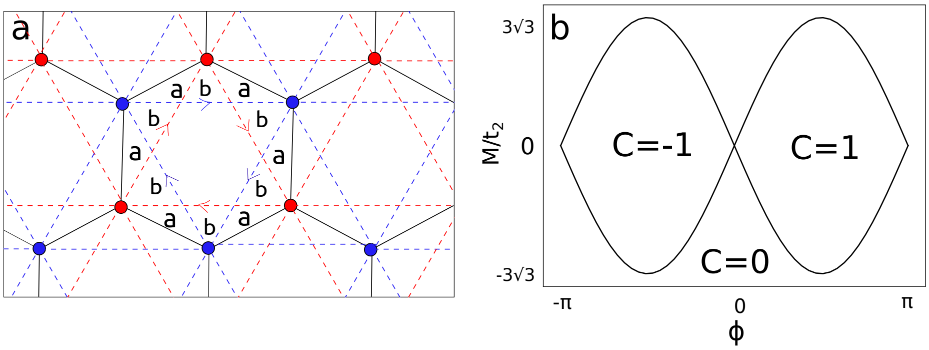

Figure 1.3: Schematic illustration of (a) graphene honeycomb lattice, where the solid (dashed) lines are for the nearest (next-nearest) neighbour hoppings. (b) Topological phase diagram with non-zero and zero Chern numbers separated by bulk-gap closing (in solid line). Figure adapted from [15].

1.2.2 Qi-Wu-Zhang model

In 2005, Qi-Wu-Zhang proposed a model to realize quantum anomalous Hall effect in semiconductors [16]. They considered a minimal, two-band model on a square lattice in the low energy range around $\mathbf{k} = 0$. The model they considered is a massive Dirac Hamiltonian given by,

$$h(\mathbf{k}) = \sum_{a=1,2,3} d_a(\mathbf{k})\sigma^a, \tag{1.12}$$

where σ's are the Pauli matrices and $\mathbf{k} = (k_x, k_y)$ is the Bloch wave vector of the electron. The two bands depends on the system considered, for example, it could be from spin or orbital degrees of freedom. By defining the unit vector $\hat{\mathbf{d}}(\mathbf{k}) = \mathbf{d}(\mathbf{k})/|\mathbf{d}(\mathbf{k})|$, the TKNN formula introduced previously becomes [16],

$$\sigma_H = \frac{e^2}{h}\frac{1}{4\pi}\int dk_x \int dk_y \hat{\mathbf{d}} \cdot \left(\frac{\partial \hat{\mathbf{d}}}{\partial k_x} \times \frac{\partial \hat{\mathbf{d}}}{\partial k_y} \right). \tag{1.13}$$

The unit vector $\hat{\mathbf{d}}(\mathbf{k})$ is a mapping from the momentum space to the unit vector in a sphere. The integrand in (1.13) is therefore, the Jacobian of the mapping $\mathbf{T}^2 \to \mathbf{S}^2$ [22, 36]. The full integration in (1.13) yields an integer multiple of the covered surface area [46]. This gives the expression $\sigma_H = Ce^2/h$ for the minimal model, where the integer C is the Chern number. It is possible to obtain non-zero values of C, by choosing the appropriate expressions for $d_a(\mathbf{k})$ around the Γ point in the Brillouin zone,

$$d_x = Ak_x,\ d_y = -Ak_y,\ d_z = M + B(k_x^2 + k_y^2), \tag{1.14}$$

where A, B and M are material-dependent parameters. When the above expressions are expanded around $\mathbf{k} = 0$, for $B = 0$, M is the Dirac mass. In the general case when $B \neq 0$, $\hat{d} = sign(M)\hat{z}$ for $k = 0$ and $\hat{d} = sign(B)\hat{z}$ for $\mathbf{k} \to \infty$. Therefore, the sign of the ratio M/B determines the topological phase. For $M/B < 0$, $\hat{d}$ points in opposite direction at $k = 0$ and $k \to \infty$, whereas for intermediate values of k, $\hat{d}$ tilts and winds around $k = 0$. Therefore, $\hat{d}$ covers the whole surface area of the unit sphere, giving $C = 1$. For $M/B > 0$, $\hat{d}$ points in the same direction at $k = 0$ and $k \to \infty$. Therefore, for other values of k, $\hat{d}$ does not have a winding number, as it first covers and then uncovers the same surface area and hence results in $C = 0$ [16]. $M/B < 0$ ($M/B > 0$) has inverted (normal) band structure, where the valence (conduction) band lies above the conduction (valence) band (see section 1.3.1), and are topologically distinct [46]. The inverted band structure supports chiral edge states (see Fig. 1.4). The topological transition between the two phases occurs at $M = 0$ when the bulk-gap closes. From the bulk-boundary correspondence, the number of edge states is equal to the Chern number.

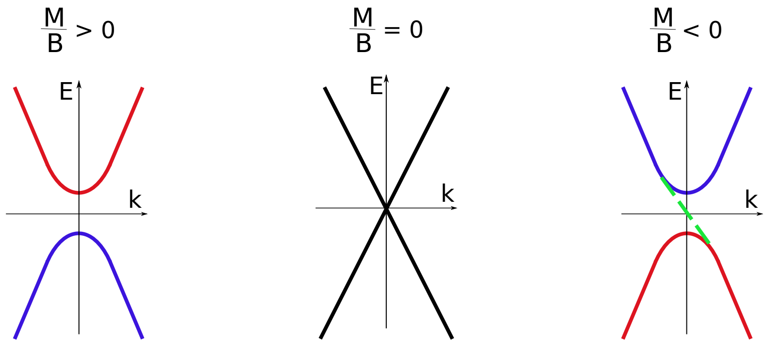

Figure 1.4: Schematic illustration when the energy band structure (a) is normal, (b) has zero bulk-gap, (c) is inverted. The inverted band structure is topologically non-trivial and supports chiral edge states (in green) on the boundary of the two-dimensional material. Figure adapted from [48].

In Haldane and Qi-Wu-Zhang models, there are no Landau levels to explain the quantization of Hall conductivity. The non-zero quantized Hall conductivity appears when time-reversal symmetry is broken and there is an associated change in the sign of mass term or band inversion is present. The model proposed by Qi-Wu-Zhang is experimentally more realistic, as it can be based on quantum spin Hall insulators (see section 1.3) with broken time-reversal symmetry (see section 1.3.2). In particular, it is known that some materials with strong spin-orbit coupling can exhibit inversion of bands. Moreover, the breaking of time-reversal symmetry could be done by using ferromagnetic insulators or magnetic doping. The change in the sign of the mass term could be acheived by varying some tunable parameter. The first successful realization of quantum anomalous effect was in Chromium doped $(\text{Bi,Sb})_2\text{Te}_3$ [17]. Various Moiré materials like twisted bilayer graphene, ABC trilayer graphene on h-BN and transition metal dichalcogenide bilayer moiré superlattices have shown quantum anomalous Hall effect [50–52]. Magnetically doped topological insulator films have also been used to realize this effect [53]. So far, the best accuracy of the observed anomalous Hall conductance in experiments is on the order of 10^{-6} [47, 54, 55]. It has been shown experimentally that as longitudinal resistance obtains a peak value, the Chern number and the associated Hall conductance changes [56].

1.3 The quantum spin Hall effect

In the above discussion, the role of spin was not considered via spin-orbit coupling. When each copy of the spin is introduced into Hamiltonian, like in (1.15), the time-reversal symmetry of the total Hamiltonian is preserved and there appears another topological state called the quantum spin Hall state[13, 57–62]. The first toy model was proposed by Kane and Mele for graphene[63]:

$$H = \begin{pmatrix} H_\uparrow(\mathbf{k}) & \lambda(\mathbf{k}) \\ \lambda^\dagger(\mathbf{k}) & H_\downarrow(\mathbf{k}) \end{pmatrix}. \tag{1.15}$$

Here $H_{\uparrow(\downarrow)}$ is the Hamiltonian introduced by Haldane but with a fixed spin [15] denoted in the subscript and λ is a matrix that couples the two spin-sectors. From time-reversal symmetry, $\lambda(\mathbf{k}) = \lambda^T(-\mathbf{k})$. Moreover, $H_\uparrow$ and $H_\downarrow$ are time-reversed copies of each other and $H_\downarrow = H_\uparrow^*(-\mathbf{k})$. It is found that, inside the energy gap opened by the spin-orbit interaction around the Fermi level, there appears a state that connects the K and K' point in the positive direction in the energy E vs k spectrum. Due to time-reversal symmetry, there also appears a state of the second spin that connects K' to K in the negative direction of k in the energy spectrum. The two edge states cross at special points in the Brillouin zone (see Fig. 1.5).

These edge states are called as *helical edge states* and appear on the edge of a two-dimensional sample while the bulk remains insulating [63]. The crossing of the edge states is facilitated by translation and time-reversal symmetry present in graphene. The crossing points are called TRIM (time-reversal invariant momenta) points in the Brillouin zone [37]. For a zigzag edged graphene nanoribbon, the crossing occurs at $k = \pi$ whereas for an armchair edge, the crossing is at $k = 0$ [63].

When $\lambda = 0$, the spin-sectors are not coupled and S_z is a conserved quantity. Each spin sector is a sub Hamiltonian that is a quantum anomalous Hall insulator (see section 1.2), and therefore a non-zero Chern number can be calculated for them. Because the spin-sectors are related by time-reversal symmetry, the Chern numbers are equal in magnitude and opposite in sign. The sum of the two Chern numbers give zero charge Hall conductance whereas the difference gives a finite and quantized

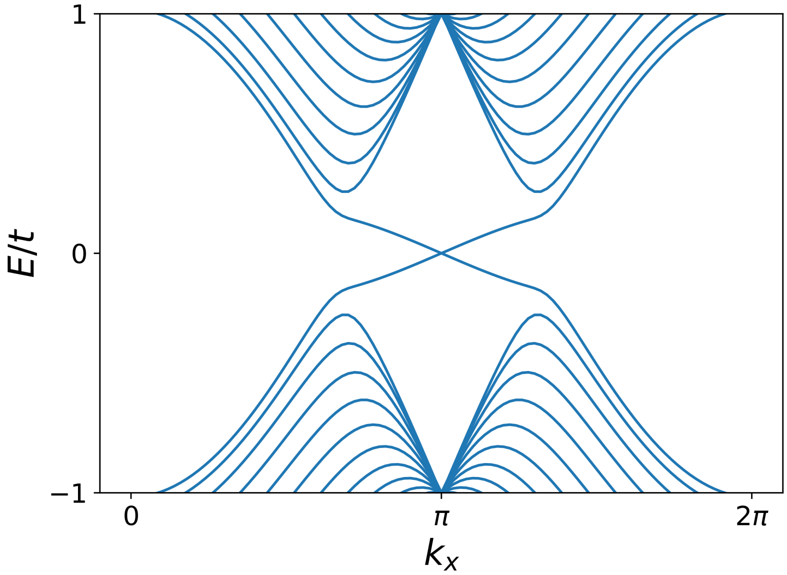

Figure 1.5: Schematic illustration of crossing of the helical edge states at $k_x = \pi$ for a graphene nanoribbon with zizag edges in quantum spin Hall phase. Figure adapted from [63].

value for spin Hall conductance. An example of this calculation is presented in the next chapter for HgTe/CdTe quantum well.

When $\lambda \neq 0$, there is coupling between the two spin-sectors. In graphene this could be due to the Rashba coupling [63], and S_z is no longer a conserved quantity. One cannot calculate the Chern number separately as in the previous case. In order to identify the topological state, a Z_2 topological invariant is calculated by Kane and Mele in a separate paper [64]. In the quantum spin Hall state, it is found that up to a certain strength, the crossing of the helical edge states was not lifted and the system remained in quantum spin Hall state [63]. This topological invariant counts the number of pairs of gapless modes on each edge. This will be discussed in more detail later.

In both cases, the importance of time-reversal symmetry is established. As long as the time-reversal symmetry is not broken, the helical edge states will cross at a TRIM point in the Brillouin zone. However, experimentally observing this topological phase in graphene is difficult because of the small energy gap ($\sim 10^{-3}$meV) opened by the very weak spin-orbit coupling in graphene [65, 66]. A small bulk-gap may allow even a weak perturbation to close the bulk-gap and destroy the edge states, so a large bulk-gap is favourable.

In an independent work, Bernevig, Hughes and Zhang (BHZ) proposed an alternative model to realize quantum spin Hall state [13]. The BHZ model, also can be thought of as two copies of the Qi-Wu-Zhang model for each spin. The helical edge states appear, when the bands are inverted, as was briefly discussed in section 1.2.2. Moreover, the model was proposed for a HgTe/CdTe quantum well, where the strong spin-orbit coupling opens a large gap in the energy band spectrum. This allows for an experimental observation of these edge states as they are protected by a large gap from the bulk states. The change in the sign of the mass term in the massive Dirac Hamiltonian for this heterostructure, is brought upon by varying the width of the quantum well. This theoretical proposal was followed by an experimental confirmation [14]. In this thesis, only BHZ like models, that can be described by a massive Dirac Hamiltonian will be considered. The BHZ model will be discussed in more detail in the next chapter for two types of quantum wells, for the cases where spin-sector coupling is absent [13] and present [60]. Below, we discuss some important properties of quantum spin Hall insulators.

1.3.1 Inverted band structure

In the BHZ model, one of the most important conditions to host the quantum spin Hall phase is to drive the system to have an inverted band structure. In the Qi-Wu-Zhang model [16], when the mass term $M > 0$, the system has a normal progression of bands, meaning that the electron-like band lies above the hole-like band, with a positive energy gap. This is adiabatically connected to a trivial band insulator where the conduction band lies above the valence around the Fermi energy. When $M < 0$, the electron like band lies below the hole like band, and this results in an energy gap with a negative sign. This is the inverted band structure and is found in materials with very strong spin-orbit coupling. The two regimes are separated by a bulk-gap closing at $M = 0$ and hence are topologically different. In the inverted band regime, the system behaves like a quantum spin Hall insulator. This will be discussed in detail in Chapter 2.

1.3.2 Time reversal symmetry

The time-reversal symmetry $\mathcal{T}$ operator for spin 1/2 particles is anti-unitary. The operator $\mathcal{T} = \tau\mathcal{K}$ is a product of a unitary operator τ and a complex conjugate operator $\mathcal{K}$. Let's say there is a state $|\psi\rangle$ with say, spin-up and it's time-reversed partner with same energy, is $|\mathcal{T}\psi\rangle$ with spin-down. When $\mathcal{T}^2 = -1$, we get $\tau\tau^* = -1$ which implies that $\tau = -\tau^T$. We have,

$$\langle\psi|\mathcal{T}\psi\rangle = \sum_{i,j}\psi_i^*\tau_{ij}\mathcal{K}\psi_j = \sum_{i,j}\psi_i^*\tau_{ij}\psi_j^* = -\sum_{i,j}\psi_i^*\tau_{ji}\psi_j^* = -\sum_{j,i}\psi_j^*\tau_{ji}\mathcal{K}\psi_i = -\langle\psi|\mathcal{T}\psi\rangle. \tag{1.16}$$

The above condition is possible only if $|\psi\rangle$ and $|\mathcal{T}\psi\rangle$ with the same energy are orthogonal to each other. This is called *Kramer's degeneracy* and the two states are called *Kramer's pair*. The counter propagating edge states that realise at the edge of the quantum spin Hall insulator is a Kramer's pair. As long as the time-reversal symmetry is protected, backscattering from disorder or interaction from one spin-up channel to the spin-down channel along the same edge is not possible as doing so would need the backscattered electron to flip its spin. Even when a TRS obeying impurity can flip the spin, it still cannot cause backscattering. Let's assume that there is an arbitrary disorder potential U_{dis} obeying time-reversal symmetry $\tau U_{\text{dis}}^T\tau^\dagger = U_{\text{dis}}$. Then the perturbation does not couple the Kramer's partners because $\langle\psi|U_{\text{dis}}\tau\mathcal{K}|\psi\rangle = 0$ i.e. the matrix element of U_{dis} between the Kramer's partners vanishes. The proof is similar as the calculation above. In other words, time-reversal symmetry is a crucial ingredient to protect helical edge states in these topological materials [64, 67, 68].

1.3.3 $\mathbb{Z}_2$ Topological invariant

As briefly mentioned before, there is a need for another topological invariant that identifies the quantum spin Hall phase when there exists a coupling between the two spin-sectors of the Hamiltonian. The closing of the bulk-gap in such materials comes with a difference in the number of Kramer's pairs of 1. This means one can use topological invariant ν which has a $\mathbb{Z}_2$ classification, meaning it can take two values which counts odd or even number of Kramer's pairs [13, 64, 69]. By relating

ν to the parity of the number of edge states nesting in the bulk-gap, we get

$$\nu = \frac{N(E)}{2} \,(\mathrm{mod}2). \tag{1.17}$$

Here $N(E)$ are the total number of energy states that crosses the Fermi energy. A more detailed discussion on the Z_2 topological invariant is presented in Chapter 2 for the Bernevig, Hughes and Zhang model.

1.3.4 Quantized conductance

A signature of odd (even) number of helical pairs along the edge for the quantum spin Hall (normal) phase is also reflected in conductance measurements. For the BHZ model, the two-terminal quantized conductance goes from 0 (no helical pair) to $2G_0$ (one helical pair) where $G_0 = e^2/h$ as the system transitions from trivial to quantum spin Hall insulator. As has been discussed, the quantum spin Hall state is characterized by odd number of helical edge states, which carry opposite spins in opposite directions. In Ref. [13], a multi-terminal setup is also proposed for additional confirmation of helical edge states.

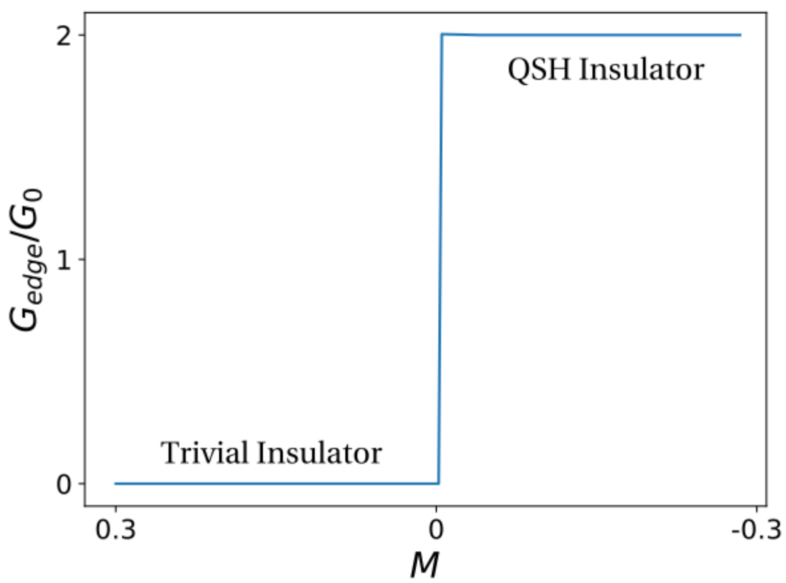

Figure 1.6: Behaviour of edge conductance in trivial and quantum spin Hall phase as a function of the Dirac mass term.

1.3.5 Experimental signatures

The proposed candidate material HgTe/CdTe by Bernevig-Hughes-Zhang to observe quantum spin Hall effect has been studied extensively [13]. Below we list experimental measurements that were carried out to confirm the properties characteristic of a quantum spin Hall insulator [14, 70–72].

When a magnetic field is applied perpendicularly to the two-dimensional sample, the features of the Landau level spectrum indicate whether the system has trivial or inverted band structure. In the normal regime, like most materials, the Landau levels shift to higher energies with increasing magnetic field. In the quantum spin Hall phase, due to the presence of an inverted band structure, the electron (hole)-like subband shifts to higher (lower) energies with increasing magnetic field. This leads to the two Landau levels to cross at some critical value of the magnetic field. The crossing of the Landau levels is characteristic of inverted band structures [14]. In order to test the presence of time-reversal symmetry that is essential for quantum spin Hall insulators, a perpendicular and in-plane magnetic field are applied. Even for weak strengths of perpendicular field, the edge conductance decreases quickly with increasing magnetic field. On the other hand, for an in-plane magnetic field, the edge conductance decreases more slowly with increasing magnetic field. The decrease of conductance demonstrates that the protection of edge states is lost due to breaking of time-reversal symmetry [14, 58, 59]. As will be discussed in the next chapter, when the spin sectors are coupled, the response of an in-plane magnetic field differs greatly from the case when the two spin-sectors are not coupled.

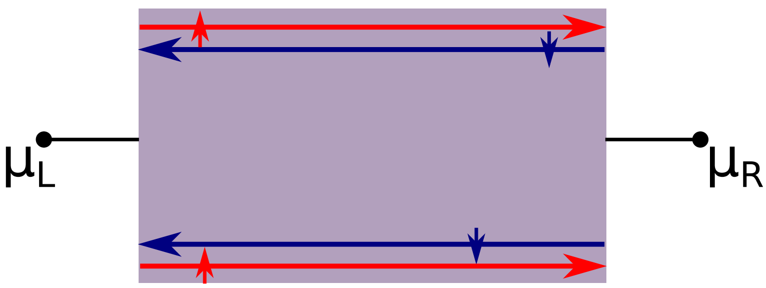

Figure 1.7: Sketch of a pair of helical edge states in a quantum spin Hall insulator. Bulk states are absent in the the figure given that in a quantum spin Hall insulator the bulk remains insulating. A two-terminal conductance measurement between μ_L and μ_R yields $G_{LR} = 2e^2/h$. Figure adapted from [13].

In the absence of magnetic fields, the presence of helical edge states is probed by measuring the edge conductance in a two terminal setup (see Fig. 1.7), the conductance measured is quantized with value $2e^2/h$ in the quantum spin Hall phase and zero conductance in the trivial phase. The argument that the contribution to the measured conductance is only from the edge states and not from the bulk is checked by measuring the longitudinal conductance by changing the width of the sample. Since, the width of the sample does not affect the measured quantized conductance, it is concluded that the bulk does not participate in the transport and only edge states do [14]. The quantized edge conductance in quantum spin Hall phase is confirmed in the presence of a disordered sample [71] or when both interactions and disorder are present [68]. The transport measurements have been performed in two and four terminal setups [73]. The current is also known to flow through the bulk of the sample while the edge conductance remains quantized [70, 72]. The edge currents have also been observed in imaging experiments [72, 74]. The dissipationless, helical edge states have only been seen in short samples [14, 70, 73, 75]. In long samples, the edge conductance takes values lower than the quantized value [14, 70, 71, 76, 77]. To understand why the edge conductance is not perfectly quantized when time-reversal symmetry is present, effect of magnetic impurities [78, 79], disorders and interactions [68, 80–85] have been considered.

1.4 Role of interactions

As mentioned before, one of the reasons for the lack of topological protection of the edge states in these materials, which is important to be studied is the effect of Coulomb interactions.

The non-interacting theory predicts that in quantum spin Hall insulators, a large magnetic field closes the bulk-gap leading to an indirect semimetal phase [86]. In contradiction to this, it was found that in the type-II quantum wells such as InAs/GaSb, the quantization was found up to a large magnetic field of 10T [70]. This suggests that interaction effects should be considered to explain such observations. Moreover, in the absence of magnetic field, it has been observed that the longitudinal resistance is linearly growing with the device length and the mean free path is also temperature independent. This is in contradiction to the topological protection of helical edge states against elastic backscattering when time-reversal symmetery is preserved. However, in the light of interaction effects that break time-reversal symmetry spontaneously, the temperature independence of the mean free path could be understood. The InAs/GaSb quantum well, is a well studied candidate to observe exciton condensation [87]. To put it simply, electrons from the conduction band and holes from the valence band can form bound states called excitons. These excitons can also form a condensate in certain conditions. Therefore, the role of excitons could be explored to study the low accuracy of the quantization observed in quantum spin Hall insulators. There are several recent experimental evidences of the presence of excitons in InAs/GaSb [88–92] and WTe_2 [93–95]. It has also been shown theoretically that excitons are important in HgTe/CdTe bilayers [96]. We will look into the role of excitons in InAs/GaSb quantum wells in more detail in Chapter 3 of this thesis.

1.5 Majorana zero modes

In solid-state systems, Majorana zero modes (MZMs) are highly localized quasiparticles with zero energy and fundamentally different from electrons and bosons. Upon an interchange of two electrons (bosons) the many-particle wavefunction acquires a factor of -1 (1). For a degenerate state of Majorana zero modes, the factor is in general a matrix, which makes these quasiparticles a manifestation of non-Abelian anyons [97–101] and their statistics is non-Abelian [102, 103]. This interesting property make the system supporting MZMs a viable candidate for topological quantum information processing. Additionally, MZMs are described by operators which are self-adjoint and square to 1 [97]:

$$\gamma = \gamma^\dagger, \implies \gamma^2 = 1, \tag{1.18}$$

$$[H, \gamma] = 0. \tag{1.19}$$

The localization of MZMs is determined from (1.19) [97]. The operator γ is considered as half a fermion, which means that two MZMs γ_1 and γ_2 can be combined to make one fermionic state $f = (\gamma_1 + i\gamma_2)/2$ with a possible occupation of zero or one [98]. The two MZMs are related by the following anti-commutation rule:

$$\{\gamma_i, \gamma_j\} = 2\delta_{ij}. \tag{1.20}$$

These quasiparticles have been theoretically shown to be present in spinless p-wave superconductors [98, 101]. More precisely, they will appear at the end of a spinless p-wave superconducting one dimensional chain and at vortices or defects of a two-dimensional p + ip superconductor (see Chapter 16 in Ref. [36] for a detailed discussion). Experimental realization of MZMs in solid state systems would confirm the existence of particles that are their own antiparticles, first proposed by Ettore Majorana [104], and allow to observe non-Abelian statistics [102, 103]. Their experimental confirmation would then pave the way for practical applications in quantum computing but also for developing fundamental theories in physics. This makes the study to realize MZMs in solid state systems an active research field in condensed matter physics.

There are some naturally occurring materials that in principle can host MZMs, but so far there are no experimental observation of their topological phase [105, 106]. Hence, the scientific community have resorted to artificially creating a spinless p-wave superconductor, which in its topological phase will host Majorana zero modes. The one-dimensional toy model is the Kiteav chain of length N [107], given by:

$$H = \sum_j \left[-t(c_j^\dagger c_{j+1} + c_{j+1}^\dagger c_j) - \mu \left(c_j^\dagger c_j - \frac{1}{2} \right) + \Delta c_j c_{j+1} + \Delta^* c_{j+1}^\dagger c_j^\dagger \right]. \tag{1.21}$$

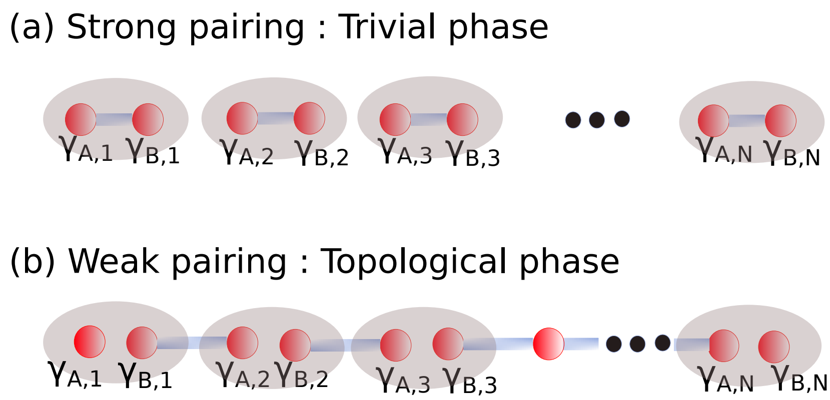

Figure 1.8: Schemtatic illustration of one-dimensional Kitaev's chain in two different topological regimes. (a) In the strong pairing, the on-site couplings dominate and there are no end states, hence is the trivial phase. (b) In the weak pairing phase, there appears unpaired MZMs at the end of the chain. The weak pairing phase becomes the topological regime. Figure adapted from [98]

.

where c and $c^\dagger$ are fermionic annhilation and creation operators respectively. Each fermionic site j can be occupied by a pair of MZMs at subsites A and B:

$$\gamma_{A,j} = c_j + c_j^\dagger,\ \gamma_{B,j} = \frac{c_j - c_j^\dagger}{i}. \tag{1.22}$$

Using the above relations, we can re-write the Hamiltonian (1.21) in terms of the Majorana operators γ. When $|\Delta| = t = 0$ and $\mu < 0$, there is strong coupling between the MZMs at subsites A and B of the same site j. When $|\Delta| = t > 0$ and $\mu = 0$, there is coupling between the MZMs at the neighbouring sites, this is also called the weak pairing regime. In the weak pairing regime, MZM are localized at the ends of the chain (see Fig. 1.8). A Z_2 topological invariant can be define which calculates the parity of the ground state. If the ground state is a superposition of even (odd) number of fermions, the parity is even (odd). In the topological (trivial) phase, the parity is odd (even) [107].

With the discovery of topological insulators, a way to capture Kitaev's toy model and realize MZMs was introduced [108–110]. These models make use of a topological insulator in proximity with an s-wave superconductor when a magnetic field is applied or the system is interfaced with a ferromagnetic insulator. The model can be considered to have the following components [98]:

$$H = H_{TI} + H_Z + H_{SC}. \tag{1.23}$$

The first component is the Hamiltonian for a topological insulator with strong spin-orbit coupling, which is needed to achieve the effective spinless p-wave superconductivity and necessary to obtain Majorana zero modes. The second Hamiltonian introduces broken time-reversal symmetry which is required to obtain unpaired localized MZMs (otherwise MZMs would necessarily come in time-reversed pairs). The third component is the Hamiltonian for an s-wave superconductor, which introduces particle hole symmetry and makes it possible to realize particles that are their own antiparticles.

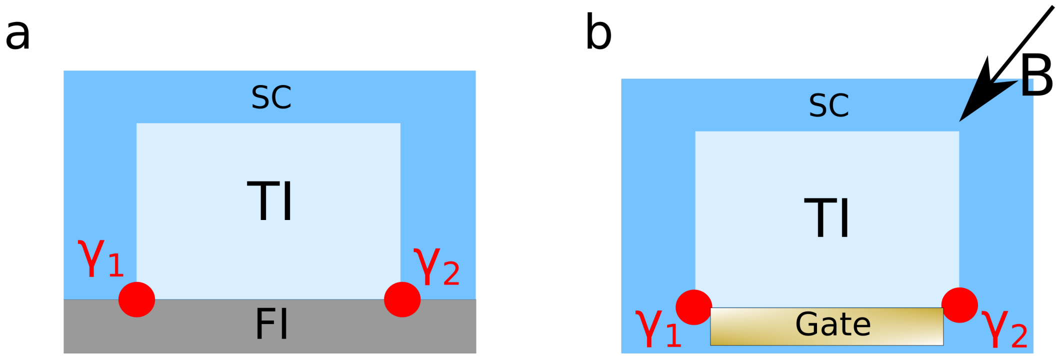

Figure 1.9: Schematic illustration of experimental setup to realize Majorana zero modes at (a) the interface of s-wave superconductor (SC), a two-dimensional topological insulator (TI) and ferromagnetic insulator (FI). At the interface of (b) s-wave superconductor (SC), two-dimensional topological insulator (TI) and a Zeeman field with electrostatic gating. [98].

Presently, there are several different indicators which help in confirming the existence of Majorana zero modes like zero-bias tunneling [111, 112], 4π Josephson effect [113, 114] and quantum interferometry methods [115]. However, realizing Majorana zero modes has not been an easy quest as it requires high quality of sample, very low temperature, high strengths of magnetic field and perfect interfacing between materials [97, 116–118]. There have been several experiments which pointed to the realization of Majorana zero modes [115, 119–123], but there still lacks an unambiguous observation of these elusive quasiparticles. Therefore, the design of a system for realization of MZMs becomes an additional motivation for our paper attached in Chapter 5.

1.6 Quantum transport theory

We present here the quantum transport theory which is used to calculate the conductance through a sample. The numerical package Kwant [124] is used to calculate bulk and edge conductance in Paper I [125]. Kwant also implements the following theoretical model to calculate conductance. Let us consider the simplest setup where the conductance through a sample is measured using two terminals. The sample is connected to two contacts through two ideal waveguides called leads, as schematically shown in Fig.1.10.

The contact is an electron reservoir which is in thermal equilibrium but have dif-

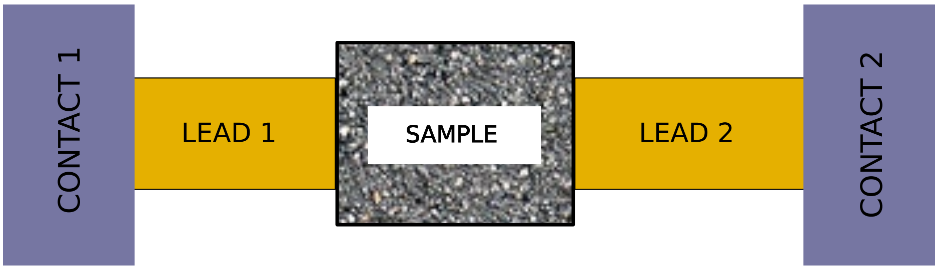

Figure 1.10: Schematic illustration of a two-terminal setup to calculate conductance through a sample. The leads here are ideal waveguides which are connected to electron reservoirs called contacts. Figure adapted from [2].

ferent value of Fermi energies, say μ_1 and μ_2 and the difference between the Fermi energies is equal to the voltage. The interface between the contact and the lead is perfect. Also, the states moving to the right (left) have thermal distribution of the left (right) contact.

When the sample is not a clean system and contains impurities, it can be represented in the form of the scattering matrix. We start by solving the Schrodinger's equation of the sample and obtaining the asymptotic wavefunctions in both directions [126]. Only the propagating waves of the wavefunctions obtained, contribute to the conductance. The proportionality coefficients that measure the amplitude of the waves that emerge from the contacts in the two leads and of the waves that are transmitted through or reflected back from the sample in each lead, are obtained. These coefficients are combined to form a scattering matrix $\hat{s}$ that has the form

$$\hat{s} = \begin{pmatrix} \hat{r} & \hat{t'} \\ \hat{t} & \hat{r'} \end{pmatrix} . \tag{1.24}$$

The *reflection* matrix $\hat{r}$ ($\hat{r'}$) contains all the electron reflections to the left (right) lead. The *transmission* matrix contains transmission of electrons through the sample. Let us first consider that there is only one open channel in the two leads. For the lead 1 that connects contact 1 and the sample, there are right-moving states that emerge from contact 1 and are partially reflected back from the sample and then there are the left-moving states that arrived from contact 2 and were partially transmitted through the sample. The probability of the reflected (transmitted) states in the lead is $R = |r|^2$ ($T' = |t'|^2$). From the unitarity of the scattering matrix it follows that $1 - R = T = T'$. The current that flows in lead 1 is,

$$I = \frac{e}{h} \int dE\, T(E) \left[f(E - \mu_1) - f(E - \mu_2) \right] , \tag{1.25}$$

where $f(E)$ is the Fermi distribution at energy E, and μ_1 and μ_2 are the chemical potentials in the left and right lead respectively. Using $\mu_1 = eV$ and $\mu_2 = 0$ (Fermi energy chosen to be 0), one easily sees from Eq. (1.25) that the voltage-dependent differential conductance $G_d(V) = dI/dV$ is given by

$$G_d(V) = \frac{e}{h} \int dE\, T(E) \frac{df(E - eV)}{dV} , \tag{1.26}$$

so that at zero temperature

$$G_d(V) = \frac{e^2}{h} T(E = eV). \tag{1.27}$$

This formula is the reason why we can probe the energy-dependent (voltage-dependent) transmission via the differential conductance. When there are more open channels in the lead, then the generalized form of the conductance is,

$$G_d(eV) = \frac{e^2}{h}\sum_{n=1}^{M} T_n(E = eV), \tag{1.28}$$

where M is the total number of open channels in the lead and T_n are the eigenvalues of the transmission matrix $tt^\dagger$ [37]. This is called the *Landauer formula*, which calculates the current across a sample in a two-terminal setup. To summarise the idea, the conductance is obtained from calculating the current flowing in a lead. The lead contains reflection and transmission coefficients of the states that are partially reflected and transmitted from (through) the sample. For a multi-lead setup, the current measured at one lead is obtained from summing over the contribution from all leads. This is known as *Landauer-Buttiker formula*. See [2, 37, 124, 126] for a detailed discussion and subtleties. A generalization of this approach to obtain differential conductance in normal-superconducting interfaces by using Andreev reflection also exists, and is called the Blonder-Tinkham-Klapwijk formula [127].

1.7 Motivation and outline

1.7.1 Motivation

So far we have looked at examples where a topological quantum phase transition takes place to give rise to interesting physics. The classification of phases in such examples relies on a topological invariant, which remains constant despite the system undergoing adiabatic changes. Typically, the topological invariant changes when the bulk-gap closes in the energy spectrum. The zero bulk-gap separates the phase diagram into states with non-zero bulk-gap and with different topological invariant. Based on the value of the topological invariant, one can identify the topological phase from a trivial one. As we have discussed, as long as no relevant symmetries have been broken, the topological phases hosts several interesting properties like a conducting edge with an insulating bulk, quantized conductance etc., which remain insensitive to perturbations. The closing of bulk-gap in these examples is akin to the act of making a hole in the topological space.

We also point out that the accuracy of the quantization of conductance measured in quantum spin Hall experiments is significantly smaller than the accuracy measured for quantum Hall or quantum anomalous Hall materials. One of the sources for such low accuracy could be many-body interactions. The study of interactions in these systems serve two purposes - first, it may provide the reason to why the perfect quantization of edge conductance is not observed in such topological insulators. Second, it allows a way for the system to achieve topological phase transition *without* bulk-gap closing. This can be understood as an effort by the system to minimize energy during the topological phase transition.

We will be looking into the application of the BHZ model to InAs/GaSb double quantum well. This material goes from a trivial state to a quantum spin Hall state as a function of front and back gate voltages or as a function of the well width. In its topological phase, the material exhibits quantized edge conductance which is not destroyed even if a magnetic field of 10T is applied for short samples. Moreover, for long samples, the longitudinal resistance is linearly increasing with the sample length for zero magnetic field. The observation of a finite mean free path constant for a wide range of temperature of 20mK to 4.2K [70–72], called for an investigation of elastic backscattering effects in this material. For this reason, the role of excitons that arise when Coulomb interactions are introduced into InAs/GaSb quantum spin Hall insulator [85] is considered. This work shows through a mean-field approach, that the excitons gives rise to an insulating phase with spontaneously broken time-reversal symmetry. This insulating phase lives in between the trivial and quantum spin Hall phase in the topological phase diagram. There are several other works that confirm that there appears signatures of excitons in quantum Hall [128–131] and quantum spin Hall systems [88, 93–95]. However, there lacks an unambiguous observation of this insulating phase that arise due to excitons in quantum spin Hall insulators. We propose an experimental setup to observe this insulating phase that leads to a topological phase transition with no bulk-gap closing.

From the discussion on the Majorana zero modes before, we know that in order to observe them, we need materials with strong spin-orbit coupling, proximity to superconductors to have particle-hole symmetry and breaking of time-reversal symmetry to lift Kramer's degeneracy to obtain well-localized Majorana zero modes. So far in the experimental setups, the time-reversal symmetry is broken by using a magnetic field or using ferromagnetic insulators. However, a strong magnetic field, which is often needed in these setups, is detrimental to superconductivity. Moreover, there is a lack of good interfacing between ferromagnetic and quantum spin Hall insulators. Therefore, an experimental observation of Majorana zero modes in two-dimensional materials is still missing. We can mitigate both the problems by utilizing the spontaneously broken time-reversal symmetry phase to realize Majorana zero modes. When superconductivity is induced through proximity to InAs/GaSb quantum well in time-reversal symmetry broken phase, we could observe the coveted Majorana zero modes. Further, we could use this system to experimentally observe Majorana zero modes as well by using a Josephson junction.

Therefore, the main questions that we address in this thesis are:

1. Can we propose an experimental setup to probe the appearance of exciton induced insulating phase with spontaneously broken time-reversal symmetry that appears in between the trivial and quantum spin Hall phase?

2. Can we use the excitons that break time-reversal symmetry to realize Majorana zero modes without using a ferromagnet or magnetic field?

3. If yes, how can one observe the Majorana zero modes experimentally?

1.7.2 Outline

In Chapter 1, we have given an overview of key theories which are important to understand quantum spin Hall effect. We have also discussed the motivation behind addressing the research problems considered in this thesis.

In Chapter 2, we will discuss the Bernevig-Hughes-Zhang (BHZ) model which describes quantum spin Hall effect in two-dimensional materials like type-I and type-II quantum wells. Even though the two materials are described by the same BHZ models, we see interesting physics that arise out of the differences between the two types of quantum wells. We look at the energy band diagrams, the choice of topological invariant and the effect of magnetic field in the two types of quantum wells.

In Chapter 3, we argue that Coulomb interactions that lead to the formation of excitons can only be observed in type-II quantum wells. We include the Coulomb interactions into the BHZ model for type-II quantum wells and discuss the findings. We proceed to show that there exists an unconventional topological transition *without* bulk-gap closing as a result of interactions in these quantum wells.

In Chapter 4, the first paper that addresses the first research question is attached along with a short summary.

In Chapter 5, the second paper that tackles the second and third research question is attached along with a summary.

In Chapter 6, we conclude the thesis by discussing the results obtained along with prospective research based on the two papers that are attached.

Chapter 2

Bernevig-Hughes-Zhang model for the quantum spin Hall effect

From the previous chapter, we are familiar that the theoretical proposal to observe quantum spin Hall effect in HgTe/CdTe quantum well [13] was also followed by its experimental confirmation [14, 73, 132]. In another work, quantum spin Hall effect was also theoretically shown to exist in InAs/GaSb quantum well [60]. This quantum well has a double well structure and was also experimentally confirmed to be a quantum spin Hall insulator [70, 77, 120]. The main difference between the two quantum wells, is that in HgTe/CdTe quantum well, the electron and hole subbands appear in the same well whereas in InAs/GaSb quantum well, the subbands appear in different quantum wells. Moreover, the spin-sectors in the Hamiltonian are not (are) coupled in HgTe/CdTe (InAs/GaSb) quantum well. Despite the differences, they both are modeled by using an effective four band model introduced in Ref. [13]. In this chapter, we will look into how the nature of the bands around the Fermi level, give rise to an inverted band structure to host quantum spin Hall phase in both the quantum wells. We also discuss the distinct observations that arise from the differences between the two quantum wells.

2.1 Quantum well structure

HgTe, CdTe, InAs and GaSb have zinc-blend structures, which are two fcc lattices interpenetrating each other with a shifted body diagonal. Because each sublattice has a different atom, the inversion symmetry is broken. For all these materials, the relevant bands close to the Fermi energy and also around the Γ point in the Brillouin zone, are an s-type band Γ_6 and a p-type band Γ_8 with $J = 3/2$ and Γ_7 band with $J = 1/2$ [13, 60, 133]. The band Γ_7 lies far away from the Fermi energy and hence its contribution is ignored while developing the effective theory for the HgTe/CdTe and InAs/GaSb quantum wells.

2.1.1 Type-I quantum well

In HgTe/CdTe quantum well, HgTe and CdTe become the well and barrier material respectively (as show in Fig. 2.1). Around the Fermi energy, CdTe has the Γ_6 band which is an s-type band and lies above the p-type Γ_8 band. On the other hand, in HgTe, the negative energy gap indicates that the Γ_8 band lies above the Γ_6 band. When the two materials come together in a quantum well, the bands combine to give rise to two effective electron and hole subbands $E1(H1)$ respectively around the Γ point. The $E1$ subband is composed of $|\Gamma_6, m_J = \pm 1/2\rangle$ and $|\Gamma_8, m_J = \pm 1/2\rangle$, and the $H1$ subband is made up of $|\Gamma_8, m_J = \pm 3/2\rangle$. $E1$ ($H1$) subbands behave as conduction (valence) subband around the Γ point and near the Fermi energy [13].
These two subbands appear in the same well material, such heterostructures are also called type-I quantum wells. When the width of the well material d is less than a critical value d_c, the $E1$ subband lies above the $H1$ subband. It has a normal band progression and is adiabatically connected to a trivial insulator. When the width of the well is above the critical value, the subband $H1$ lies above $E1$ subband. This is the inverted band structure which hosts quantum spin Hall phase (see Fig. 2.1). Since the two phases are topologically distinct, there is necessarily a bulk gap-closing, which occurs when the width of the well is equal to the critical width d_c. This phase transition is possible because the Dirac mass term in the Hamiltonian

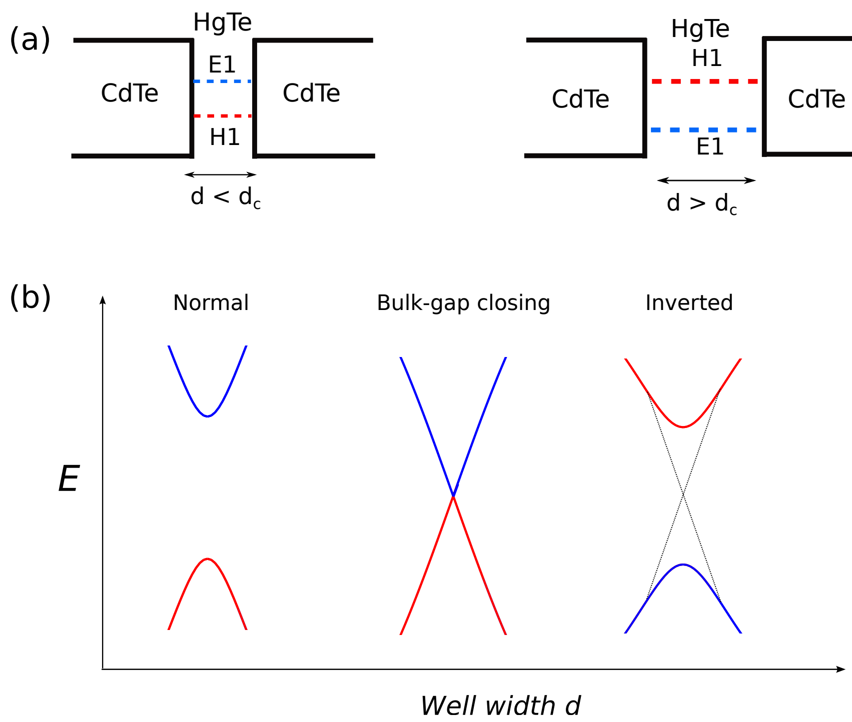

Figure 2.1: Schematic illustration of a HgTe/CdTe (a) quantum well and (b) energy band progression around Γ point as a function of well width. The quantum spin Hall phase exists when there is an inverted band structure. In this phase, there will appear helical edge states (dashed lines) in the edge spectrum. Figure adapted from [13].

changes sign after the bulk gap closing. The Dirac mass term is controlled in an experiment through the width of the well [13].

2.1.2 Type-II quantum well

This is a double quantum well structure, where there are two well materials, InAs and GaSb while the barrier material is AlSb. Just like in HgTe/CdTe quantum well, the $E1$ subband becomes the conduction band. This subband is formed in InAs and lies below the valence band $H1$, which is formed in GaSb (as shown in Fig. 2.2). The key difference in the quantum well is the separation of electron and hole like bands in different well materials. These quantum structures are also called type-II quantum wells or electron-hole bilayers. By varying the well width, below (above) a critical value of the width d_c, $E1$ ($H1$) subband lies above (below) $H1$ ($E1$) subband. This means just like the type-I quantum well, the system has normal or inverted band structure depending on the width of the well. In the inverted regime, the system be-

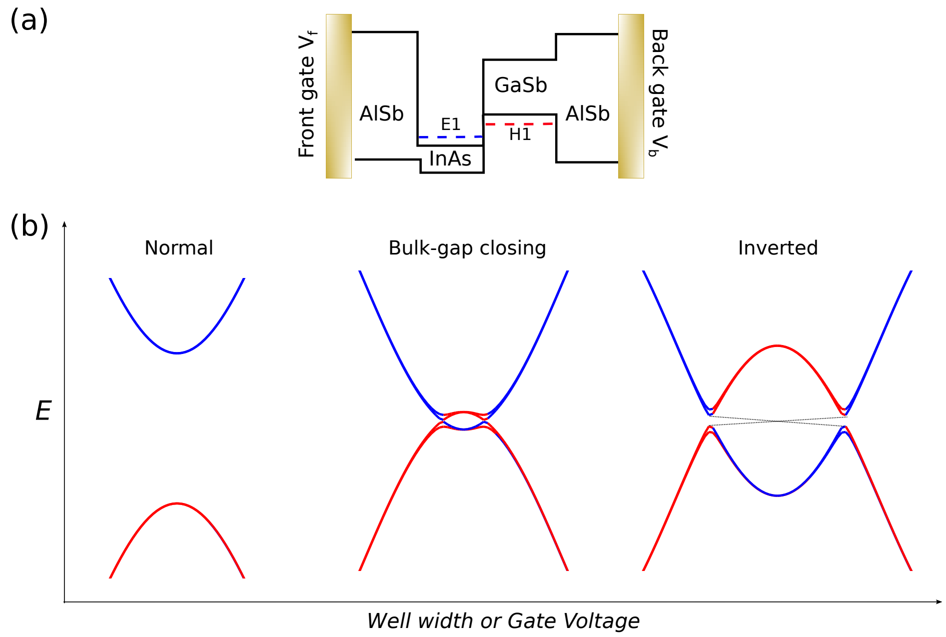

Figure 2.2: Schematic illustration of (a) quantum well structure of InAs/GaSb with Al/Sb as barrier material and (b) energy band progression as a function of well width or gate voltages. A front and back gate voltage is applied to continuously tune the quantum well from normal to inverted band structure. In the inverted regime, the system is in quantum spin Hall phase with helical edge states (dashed lines) will appear. Figure adapted from [60].

comes a quantum spin Hall phase (see Fig. 2.2). Because the two subbands are also in different materials, they are weakly coupled compared to type-I quantum well. Hence, it is possible to access them separately through front and back gate voltages [60]. The experimental realization for tuning the bands via gate voltages also exist [134]. Therefore, the Dirac mass term in these quantum wells can change as a function of well-width as well as gate voltages [60, 87, 135]. This is an advantage over the type-I quantum wells, as the bands can be continuously tuned from trivial to topological through gate voltages.

2.2 Non-interacting BHZ model

The presence of spin makes the subbands doubly degenerate, and along with time-reversal and inversion symmetry considerations, an effective four band model was proposed in Ref. [13]. The same model could also be used to describe type-II quantum wells [60]. Therefore, the general Hamiltonian for both the quantum wells becomes:

$$H_0 = \big(E_G - \frac{\hbar^2 k^2}{2m}\big)\tau_z\sigma_0 + Ak_x\tau_x\sigma_z - Ak_y\tau_y\sigma_0 + \Delta_z\tau_y\sigma_y, \tag{2.1}$$

where τ's and σ's are the Pauli matrices in the electron-hole and spin basis respectively. The parameters in this single-particle Hamiltonian E_G, $\frac{\hbar^2}{2m}$ and A correspond to M, B and A parameters of the BHZ model respectively [13]. The terms proportional to C and D, and the k dependent structure inversion asymmetry [136] terms are ignored because they do not contribute qualitatively in understanding the quantum spin Hall phase [60, 85]. The term, A is the tunnelling parameter that couples electrons and holes, E_G is the gap between $E1$ and $H1$, it also controls electron-hole density, m is the effective mass that is assumed equal for both electrons and holes and Δ_z is bulk inversion asymmetry term that mixes the two spin sectors.

As has been already discussed before, a quantum spin Hall insulator can be thought of as two copies of quantum anomalous Hall insulator. This means, each spin-sector in the Hamiltonian, if not coupled, becomes a quantum anomalous Hall insulator with a fixed spin. The two spin copies are then related through the time-reversal symmetry. The spin-orbit coupling in each spin-sector acts as a time-reversal symmetry breaking term. This allows us to calculate a Chern number for each spin-sector (shown later). The spin-orbit coupling in the Hamiltonian is given by the tunneling term A, which describes the hopping from s to p orbitals.

2.3 Symmetries of the system

2.3.1 Inversion symmetry

The bulk inversion symmetry for the Hamiltonian in (2.1) is given by,

$$\tau_z\sigma_0 H_0(-\mathbf{k})\tau_z\sigma_0 = H_0(\mathbf{k}). \tag{2.2}$$

The only term that breaks this symmetry is the Δ_z term. In type-I quantum well, the lack of inversion center in the lattice structure, weakly breaks the inversion symmetry. However, in developing the theoretical model, this symmetry can be assumed to be present if the magnitude of Δ_z is considerably small compared to the tunneling term, which is the case in type-I quantum wells. In type-II quantum wells, the lattice structure as well the quantum well structure breaks this symmetry. Therefore, the presence of bulk-inversion asymmetry cannot be as easily ignored.

2.3.2 Rotation symmetry

If the quantum well is grown along the z-axis, then the rotation symmetry about this axis by 180 degrees, is a true symmetry of the system. It is given by

$$\tau_z \sigma_z H_0(-\mathbf{k}) \tau_z \sigma_z = H_0(\mathbf{k}). \tag{2.3}$$

Every term in the Hamiltonian $H_0(\mathbf{k})$ obeys this symmetry and both spin and position space is being rotated simultaneously.

2.3.3 Time-reversal symmetry

The time-reversal symmetry for the system is defined as,

$$\tau_0 \sigma_y H_0^T(-\mathbf{k}) \tau_0 \sigma_y = H_0(\mathbf{k}). \tag{2.4}$$

The Hamiltonian (2.1) obeys this symmetry. The time-reversal symmetry in the Hamiltonian establishes a connection between two spin-sectors of the Hamiltonian.

2.4 Model parameters

The values of the parameters chosen here are scaled by E_0 and d_0 where $E_0 = \hbar^2/2md_0^2 = e^2/4\pi\epsilon\epsilon_0 d_0$. E_0 is the exciton binding energy and d_0 is the exciton Bohr radius. This choice of scaling becomes relevant when Coulomb interactions will be considered in type-II quantum wells in the next chapter.

In reality, the bulk inversion asymmetry term is also present in type-I quantum wells,

Model parameter	HgTe/CdTe	InAs/GaSb
A/E_0d_0	1.2	0.06
$B = \hbar^2/2m$	0.5	0.5
Δ_z/E_0	0	0.02

Table 2.1: Table of parameter values used for the calculations present in this thesis for HgTe/CdTe and InAs/GaSb. Table adapted from [133].

but the magnitude of the tunneling term A is so large compared to Δ_z, that Δ_z can be neglected in the Hamiltonian [13, 62, 133]. For the numerical calculations performed here, the Δ_z term in type-I quantum well is zero. In type-II quantum wells, the separation of electron and hole subbands in different materials, reduces the magnitude of the tunneling term A. In this case, both Δ_z and A have comparable magnitudes.

In this thesis, we will only consider the momentum-independent bulk inversion asymmetry Δ_z term. This assumption greatly simplifies our calculations without affecting the closing of the bulk gap at finite k for these bilayer systems [85, 125, 137].

2.5 Effect of bulk inversion asymmetry Δ_z term

In the following subsections, we will look at the energy spectrums of type-I and type-II quantum wells, to study the topological phase transition. We will use the model parameter values in Table. (2.1). We will study the properties of the quantum wells as a function of E_G/E_0, which is the Dirac mass term and can be tuned in experiments. The other parameters are constant and take the values given in Table 2.1. To calculate the edge spectrum, a ribbon of finite width along the y direction and infinite along the x direction is considered.

2.5.1 Type-I quantum well

In the calculations presented here, when $E_G/E_0 < 0$ ($E_G/E_0 > 0$), the system has a normal (inverted) band progression, the electron (hole) subband is above the hole (electron) subband (see Fig. 2.1). At $E_G = 0$, the bulk-gap closes at Γ point (see Fig. 2.1). In the inverted (normal) phase, the system becomes a quantum spin Hall (trivial) insulator with a non-zero bulk gap at Γ point. In the quantum spin Hall phase, there appears edge states with spin-momentum locking, which intersect at the Γ point. However, in the trivial phase, there are no edge states. This is seen in the edge spectrum presented in Fig. 2.3. At $E_G = 0$, the bulk-gap closes.

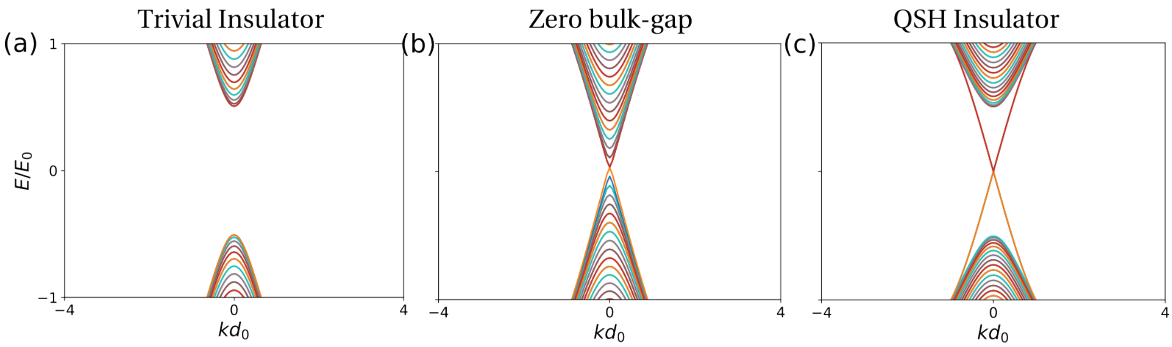

Figure 2.3: Topological phase transition in type-I quantum well when $\Delta_z = 0$ as see through the edge spectrum. In the quantum spin Hall phase, the helical edge states cross at Γ in the Brillouin zone.

As discussed before type-I quantum wells also have bulk inversion asymmetry, but because the tunneling term is so strong, the role of Δ_z term could be neglected [13, 14, 138]. We check this statement by considering $\Delta_z = 0.04E_0$ in (2.1):

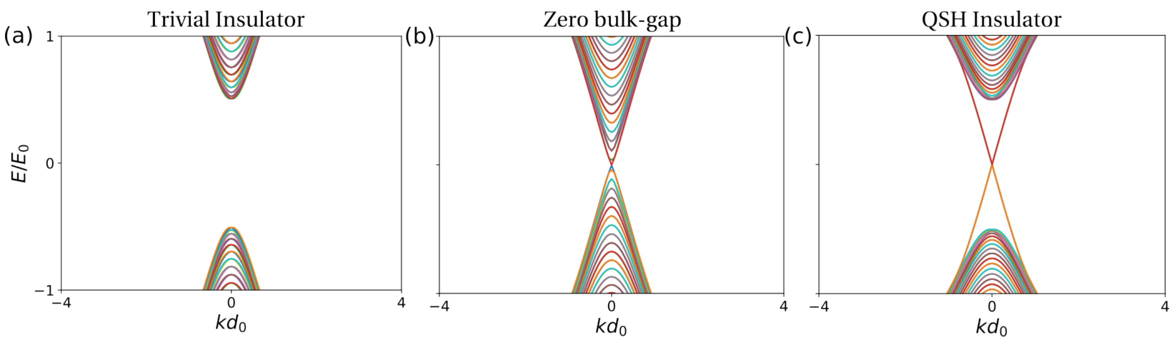

Figure 2.4: Topological phase transition in type-I quantum well when $\Delta_z \neq 0$ as seen through the edge spectrum. We notice that due to the large tunneling term A, the Δ_z term does not affect the phase transition. In the quantum spin Hall phase, the helical edge states cross at Γ in the Brillouin zone.

2.5.2 Type-II quantum well

The bulk-inversion asymmetry is naturally present in type-II quantum wells because of the lattice and quantum well structure. Moreover, the tunneling term is also small in type-II quantum wells. Hence the bulk-inversion asymmetry term cannot be neglected like before. The k independent bulk inversion asymmetry term Δ_z, couples the spin sectors but does not break the time-reversal symmetry, since the coupling is not between the Kramer partners. Therefore, it will not destroy the edge states in quantum spin Hall phase, unless it is sufficiently large and closes the bulk-gap [62]. For $E_G > 0 (< 0)$, this case exhibits the inverted (normal) regime (see Fig. 2.2). The important difference is that the bulk gap closes at a finite value of $E_G/E_0 = \frac{\Delta_z^2 d_0^2}{2A^2}$ and at a finite value of the wave vector k_{cross} [60, 77]. In the edge spectrum in Fig. 2.5, we see that in the quantum spin Hall (trivial) phase, there are (no) helical edge states that cross at Γ point.

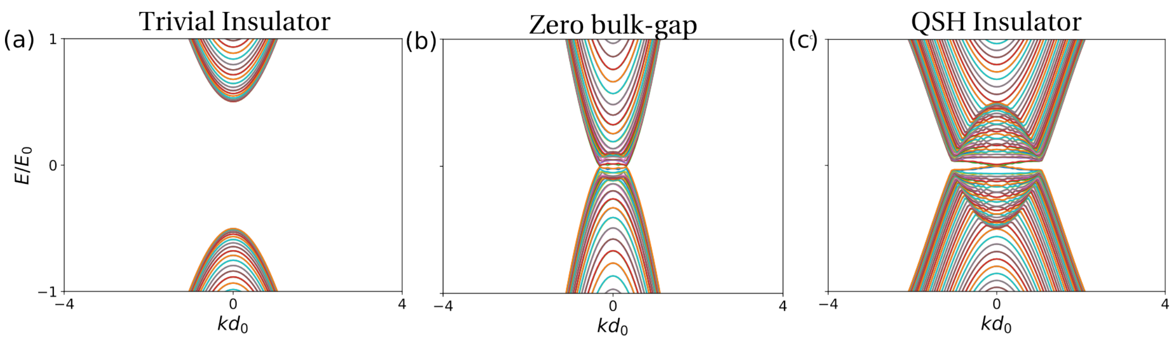

Figure 2.5: Topological phase transition for type-II quantum wells when $\Delta_z = 0.02$ as seen through the edge spectrum. The bulk-gap closes for a finite value of kd_0 and *not* at the $Gamma$ point in the Brillouin zone.

2.6 Effect of mass asymmetry

In reality, there is always a mass asymmetry between electrons and holes, that is $m_e \neq m_h$, the Hamiltonian can be written as:

$$H_0 = (\frac{\hbar^2 k^2}{2m_e} - E_{G_e})\frac{1}{2}(\tau_0 + \tau_z)\sigma_0 + (E_{G_h} - \frac{\hbar^2 k^2}{2m_h})\frac{1}{2}(\tau_0 - \tau_z)\sigma_0 + \tag{2.5}$$

$$Ak_x\tau_x\sigma_z - Ak_y\tau_y\sigma_0 + \Delta_z\tau_y\sigma_y, \tag{2.6}$$

where $E_{G_e} = \frac{2m_{\text{eff}}}{m_e} E_G$ and $E_{G_h} = \frac{2m_{\text{eff}}}{m_h} E_G$ with $1/m_{\text{eff}} = 1/m_e + 1/m_h$. The exciton binding energy and radius now becomes,

$$E_0 = \frac{\hbar^2}{2m_{\text{eff}} d_0^2} = \frac{1}{4\pi\epsilon\epsilon_0} \frac{e^2}{d_0}. \tag{2.7}$$

When $m_e = m_h = m$ and $m_{\text{eff}} = m/2$, and we recover the equations we considered in the Hamiltonian (2.1). We check the effect of mass asymmetry on the topological transition when $m_e/m_h = 0.84$. There is only a small effect due to the mass asymmetry in the dispersion of the electron and hole bands. We calculate the edge spectrum for type-I and type-II and see that the topological transition is not affected by the change in effective masses of electrons and holes (see Fig. 2.6).

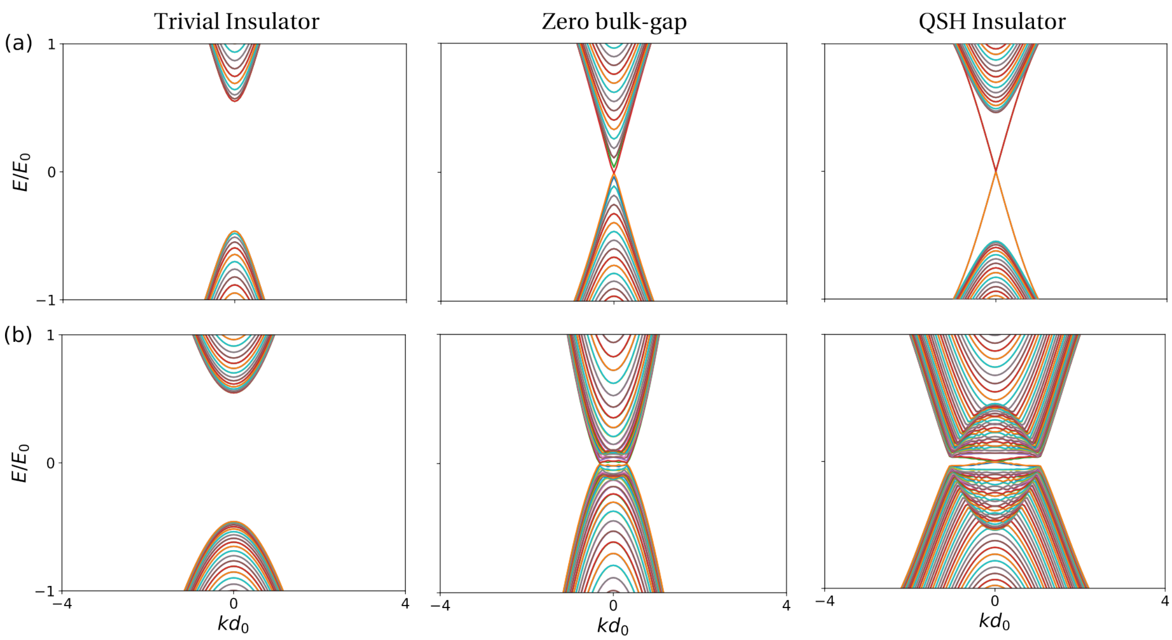

Figure 2.6: Topological phase transition with $m_e/m_h = 0.84$ for (a) Type-I quantum well when $\Delta_z = 0$ and (b) type-II quantum well when $\Delta_z = 0.02$. The gap closes at Γ if $\Delta_z = 0$ and at $E_G/E_0 = \frac{\Delta_z^2 d_0^2}{2A^2}$ and non-zero kd_0 if $\Delta_z \neq 0$. The mass asymmetry has no effect on the topological phase transition.

2.7 Topological Invariant

In the previous chapter, we discussed that a topological phase is identified by calculating a topological invariant [69]. Below we look into the choice of topological invariant when the spin sectors are (are not) coupled in the the Hamiltonian in (2.1).

2.7.1 Spin Chern topological invariant when $\Delta_z = 0$

The effective four band model for type-I quantum well, the rotation symmetry along the growth axis, inversion symmetry and time-reversal symmetry are preserved, which means that there is no coupling between the two spin sectors. Since the spin-sectors are independent of each other, the perpendicular component of the spin S_z along the growth axis z is a conserved quantity. This means, for each 2×2 spin sector of the Hamiltonian, the Chern number can be calculated like it is calculated for the quantum anomalous Hall phase. This is possible because the spin-orbit coupling in each spin-block, which is the term proportional to A, acts as a time-reversal symmetry breaking term.

The Chern number is an integer and is equal to the Hall conductance of the filled bands. It is calculated when the system is gapped. Since the two spin-sectors are related by time-reversal symmetry, the Hall conductance of each spin-sector will be related through $\sigma_{xy}(H(k)) = -\sigma_{xy}(H^*(-k))$, where $H(k)$ ($H^*(-k)$) are the spin-up (down) sectors [13]. The Hall conductance can be obtained from calculating the Berry connection and integrating over the full Brillouin zone. Each spin-sector is a two-level Hamiltonian, which can be written as $H(\mathbf{k}) = \mathbf{d}_i \cdot \sigma_i$. Here σ_i and d_i are the Pauli matrices and components of the Hamiltonian respectively. The eigenvalues of this Hamiltonian will be $\pm d$ where $d = \sqrt{d_1^2 + d_2^2 + d_3^2}$ and the eigenvectors will be:

$$\psi_- = \frac{1}{\sqrt{2d(d+d_3)}} \begin{pmatrix} -d_1 + id_2 \\ d + d_3 \end{pmatrix}, \ \psi_+ = \frac{1}{\sqrt{2d(d+d_3)}} \begin{pmatrix} d + d_3 \\ d_1 + id_2 \end{pmatrix} \tag{2.8}$$

Since, the Chern number is calculated from the filled bands, the Berry potential A_i and Berry connection Ω_{xy} will be:

$$\begin{aligned} \mathcal{A}_i &= i \langle \psi_- | \partial_{k_i} | \psi_- \rangle = \frac{-1}{2d(d+d_3)} \left[d_2 \partial_i d_1 - d_1 \partial_i d_2 \right], k_i := k_x, k_y \\ \Omega_{xy} &= \frac{\partial \mathcal{A}_y}{\partial k_x} - \frac{\partial \mathcal{A}_x}{\partial k_y} \end{aligned} \tag{2.9}$$

The Hall conductance for each spin-sector can be obtained using:

$$\sigma_{xy} = \frac{e^2}{h}\frac{1}{2\pi}\int\int dk_x dk_y \Omega_{xy} \tag{2.10}$$

For the spin $\uparrow$ sector of the Hamiltonian H_0, the components are $d_1 = Ak_x$, $d_2 = Ak_y$ and $d_3 = E_G - B(k_x^2 + k_y^2)$. The Berry potential and the curvature becomes:

$$\begin{aligned}
\mathcal{A}_x &= \frac{-A^2 k_y}{2\sqrt{A^2k^2 + (E_G - Bk^2)^2}\left(\sqrt{A^2k^2 + (E_G - Bk^2)^2} + (E_G - Bk^2)\right)}, \\
\mathcal{A}_y &= \frac{A^2 k_x}{2\sqrt{A^2k^2 + (E_G - Bk^2)^2}\left(\sqrt{A^2k^2 + (E_G - Bk^2)^2} + (E_G - Bk^2)\right)}
\end{aligned} \tag{2.11}$$

$$\Omega_{xy} = \frac{A^2(Bk^2 + E_G)}{2\left(A^2k^2 + (E_G - Bk^2)^2\right)^{3/2}} \tag{2.12}$$

Substituting (2.12) in (2.10), we get,

$$\sigma_{xy} = \frac{e^2}{h}\frac{1}{2\pi}\int\int dk_x dk_y \frac{A^2(Bk^2 + E_G)}{2\left(A^2k^2 + (E_G - Bk^2)^2\right)^{3/2}} \tag{2.13}$$

After performing the integration from $-\infty$ to ∞, for negative valued E_G, the Chern number and the Hall conductance becomes zero. For positive values of E_G and spin-up sector, we obtain $\sigma_{xy}(\uparrow) = 1e^2/h$ with Chern number $n_\uparrow = 1$. From the time-reversal symmetry, we get for the spin-down sector, $\sigma_{xy}(\downarrow) = -1e^2/h$ and Chern number $n_\downarrow = -1$. The spin Chern invariant is give by $n_\uparrow - n_\downarrow = 2$, which gives the spin Hall conductance as $\sigma^s_{xy} = 2e^2/h$ (see Fig. 2.7). The sum of the two Chern numbers is related to the charge Hall conductance and is $n_\uparrow + n_\downarrow = 0$. At $E_G = 0$, the bulk-gap closes and divides the phase diagram into trivial (quantum spin Hall) phase for $E_G < 0 (E_G > 0)$.

We can also observe the bulk-gap closing from the lattice Hamiltonian. This can be obtained by replacing $k_i \to \sin k_i$, $k_i^2/2 \to (1 - \cos k_i)$ in the continuum Hamiltonian,

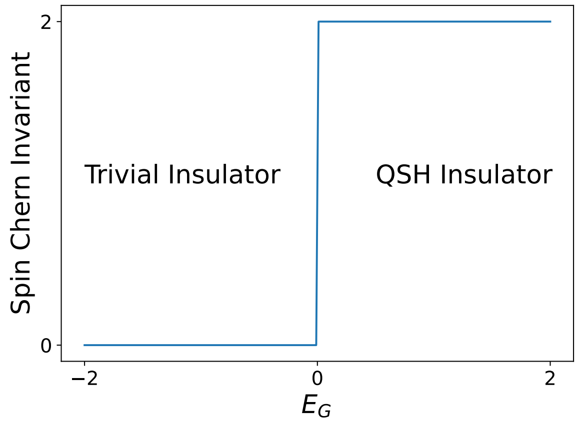

Figure 2.7: Spin Chern invariant calculated as a function of E_G. In trivial (quantum spin Hall) phase, the value of the invariant is zero (two). The value of edge conductance is equal to the spin Chern invariant in units of e^2/h.

where $k_i := k_x, k_y$. The lattice Hamiltonian becomes [13],

$$\begin{aligned} d_1 + id_2 &= A\left(\sin k_x + i\sin k_y\right) \\ d_3 &= -2B\left(2 - E_G/2B - \cos k_x - \cos k_y\right) \end{aligned} \tag{2.14}$$

The energy gap for this model is

$$E_{\text{gap}} = 2\sqrt{A^2(\sin^2 k_x + \sin^2 k_y) + 4B^2(2 - E_G/2B - \cos k_x - \cos k_y)^2} \tag{2.15}$$

which gives zero energy gap at $(k_x, k_y) = (0,0), (0,\pi), (\pi,0), (\pi,\pi)$ for values of $E_G/2B = 0, 2$ (for both $(0,\pi)$ and $(\pi,0)$) and 4 respectively, which are the transition points in the Brillouin zone.

In this chapter we are studying the topological transition that occurs as a result of bulk-gap closing at Γ point (or close to this point for $\Delta_z \neq 0$). Hence, the spin Chern invariant in the range $E_G < 0$ (trivial) and $0 < E_G/2B < 2$ (quantum spin Hall) in the lattice Hamiltonian will be relevant [13].

2.7.2 Z_2 topological invariant when $\Delta_z \neq 0$

When $\Delta_z \neq 0$, the spin-rotation symmetry breaks as Δ_z couples the two spin sectors. S_z is no longer a conserved quantity, and the spin Hall conductance is no longer quantized. As the time-reversal symmetry is still preserved, there will appear helical edge states as long as the bulk-gap is not closing.

The distinction between the different topological phases appears in the number of pairs of edge states that appear and in the way they behave in the energy gap in the two phases. In the trivial phase, the edge states typically do not cross the energy gap, and they always appear in an even number of pairs at each energy. This allows for elastic backscattering and localization of edge states. In the quantum spin Hall phase, the edge states appear in odd number of pairs and cross the energy gap. Since the time-reversal symmetry is preserved, these states are robust against weak perturbations, and therefore single-plarticle elastic backscattering is forbidden.

A quantized spin Hall conductance is not always a marker of the quantum spin Hall effect. This is argued by considering a cylinder with circumference L and by adiabatic introduction of a magnetic flux through the cylinder. A weak electric field appears along the circumference. When the rate of spin accumulation is calculated by utilizing a similar argument as in the Laughlin pump [139], the trivial phase has zero spin accumulation as the edge states are localized, whereas the quantum spin Hall system has a non-zero spin accumulation due to the particle-hole pair (whose spins do not compensate each other) that appears at the Fermi energy, which contributes to the spin Hall conductance. The spin accumulation is a robust property of quantum spin Hall effect, even though the spin Hall conductance is not quantized unless the particle and hole carry opposite spins [64]. Kane and Mele emphasize that the *quantum* does not refer to *quantized* in the context of quantum spin Hall insulators [64].

Since, the spin-sectors cannot be treated independently as was done in the case before, a new topological invariant that captures the distinct phases is required. The time-reversal symmetry operator $\mathcal{T}$, divides the Hamiltonian H_0 and the occupied energy bands $|\psi(\mathbf{k})\rangle$ into two subspaces. In the even subspace, the occupied bands, $|\psi_1\rangle$ and $|\psi_2\rangle$, span the same space as $\mathcal{T}\psi_1$ and $\mathcal{T}\psi_2$. Hence, the transformation matrix between the pairs of states is unitary. In the odd subspace, the $\mathcal{T}|\psi_1\rangle$ and $\mathcal{T}|\psi_2\rangle$ span the space of the unoccupied bands $|\psi_3\rangle$ and $|\psi_4\rangle$. The transformation matrix between $|\psi_1\rangle$ and $|\psi_2\rangle$ and $\mathcal{T}|\psi_1\rangle$ and $\mathcal{T}|\psi_2\rangle$ is now not unitary and can be zero. The aim is to find the region in $\mathbf{k}$, where the odd subspace occurs. This can be done by considering the overlap between $|\psi_i\rangle$ and $\mathcal{T}\,|\psi_j\rangle$. We get a single complex number that give this information through the Pfaffian:

$$P(\mathbf{k}) = \mathrm{Pf}[\langle\psi_i(\mathbf{k})|\mathcal{T}|\psi_j(\mathbf{k})\rangle] \tag{2.16}$$

If the occupied bands belongs to the even subspace, $|P(\mathbf{k})| = 1$ and if it belongs to the odd subspace, then $P(\mathbf{k}) = 0$. There will always be a pair of zeros that occur at $\pm\mathbf{k}^*$ points in the Brillouin zone because of time-reversal symmetry. They will not occur at time-reversal invariant momenta or TRIM points because $P(\mathbf{k}) = 1$ necessarily at these points. The Z_2 topological invariant is calculated by counting the number of zeros when the system is gapped, as the Pfaffian is undefined for zero bulk gap. In the trivial (topological) phase, there are even (odd) number of pair of zeros. As the Hamiltonian H_0 has an additional two-fold rotational symmetry, there are lines instead of points, where the zeros occur, the zeros will lie on a curve enclosing the time-reversal invariant point, which in this case is Γ (see Fig. 2.8).

The Z_2 topological invariant ν is also related to the number of edge states through the formula:

$$\nu = N(E) \mod 2, \qquad N(E) = N_+ + N_-, \tag{2.17}$$

where N_+ and N_- are the edge states moving in opposite directions to each other. Since, the number of helical edge states in the trivial and quantum spin Hall phase will differ by an odd number. The topological invariant ν is always 0 or 1, which counts the modulo 2 of the number of helical pairs that appear on the edge of the material. In the quantum spin Hall (trivial) phase, there always appear only odd (even) number helical edge states.

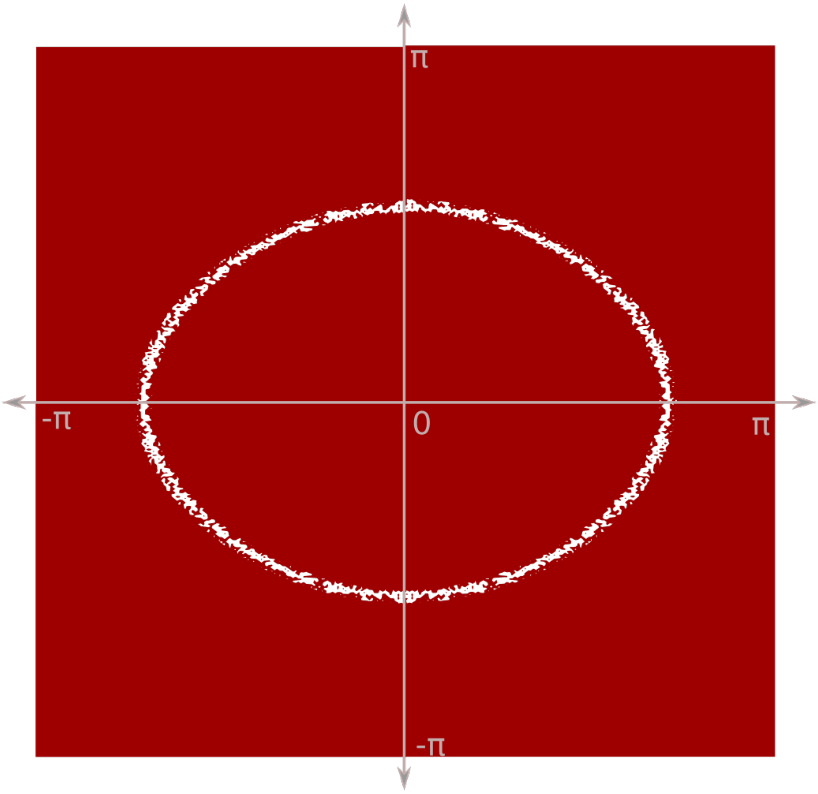

Figure 2.8: The zeros of $P(k)$ lying on a curve enclosing the Γ point, when the system is in quantum spin Hall phase.

2.8 Effect of magnetic field

Even though qualitatively, type-I and type-II quantum wells behave similarly when there is no magnetic field. The two systems respond differently to an externally applied magnetic field. Below we discuss the effect of magnetic field, and also consider the role of disorder when considered additionally.

2.8.1 Perpendicular magnetic field

Type-I quantum well: A type-I quantum well in its inverted regime supports helical edge states, which are counter propagating pseudo spin states that appear along the edges of a two-dimensional sample (or the *helical edge states*). When a magnetic field is applied, the time-reversal symmetry breaks, and a gap opens in the helical edge states. For small values of the magnetic field, there is a small edge gap and the edge transport can still be observed. Increasing the magnetic field can close the bulk-gap and give a non-zero Chern number. In other words, for a critical value of a magnetic field, the bulk-gap closes and the quantum spin Hall gives way to a quantum Hall phase [140–143]. If the Landau level spectrum is observed, there is only one Landau level from the electron and hole band each, that appear inside the bulk-gap. The value of the bulk gap is measured when there is no magnetic field applied. This is because the value of the gap is maximum when there is zero magnetic field for the inverted band structure. In the inverted regime, as the magnetic field is increased, the gap decreases [144, 145]. In this case, there appears crossing of the Landau levels from the $E1$ and $H1$ subband at a critical value of the magnetic field B_c [146]. The main contribution of the perpendicular magnetic field in this material is the orbital effect. The energy gap opening due to the Zeeman effect is less than a 1 meV [138].

Role of disorder: In normal band progression, increasing disorder decreases the band gap [147]. However, in inverted band structure, the band gap increases with increasing disorder. This means, in the presence of strong disorder, it requires a large magnetic field to close the band gap and the system to go from quantum spin Hall to quantum Hall state. In other words, the helical edge states remain robust for a large value of disorder strength.

Type-II quantum well: The type-II quantum well also is a quantum spin Hall insulator. In its inverted regime, when the magnetic field is increased, the gap between the electron and hole subbands decrease and cross each other at a critical magnetic field B_c. But, unlike the type-I quantum well, it does not become a quantum Hall insulator after this critical field. Due to the weak coupling between the electron and hole subbands, compared to the type-I quantum well, there are two more Landau levels that appear inside the bulk gap [146]. This leads to two separate crossing of the Landau levels at B_c' and B_c. From B_c' to B_c, there exists a quasi-metallic state, where there is bulk conduction [146]. At B_c, the system becomes a quantum Hall insulator with chiral edge states and insulating bulk. When the Zeeman effect is considered, there again exists a bulk-conducting region [146]. In the presence of electron-electron interactions, it has been observed that the Landau levels do not cross because of exciton condensation [148].

Role of disorder: In the case of type-II quantum wells, it is observed that as disorder increases, the critical value of magnetic field B_c' for which bulk conduction appears becomes smaller. This widens the $B_c' \lesssim B \lesssim B_c$ region, thereby reducing the robustness of helical edge states. This behaviour is very different when compared to type-I quantum well, when disorder is introduced [146].

2.8.2 In-plane magnetic field

Type-I quantum well: The in-plane magnetic field in type-I quantum wells such as HgTe/CdTe only contribute to a Zeeman splitting and there is no observation of orbital effect.

Zeeman Effect: The Zeeman splitting leads to the opening of a small gap in energy of the order less than 1 meV.

Type-II quantum well: Preserving time-reversal symmetry is crucial for the protection of helical edge states in quantum spin Hall insulators. In InAs/GaSb, an in-plane magnetic field of 10T or more is shown to not destroy these edge states [70, 72].

Though the behaviour of these bilayers in the presence of perpendicular magnetic field is still somewhat understood, the persistence of edge states in the presence of large values of in-plane magnetic field is not. In Ref. [149], it is shown that, the spatial separation of electron and hole bands allows a non-zero magnetic flux between the two layer. This results in an orbital effect in InAs/GaSb which dominate the Zeeman splitting.

Orbital Effect: In the bulk spectrum, the main effect of the orbital effect is to shift the electron and hole bands by some amplitude, $\pm\mathbf{k}_\mathrm{M}$, in $\mathbf{k}$-space respectively. The shift in the momentum $\mathbf{k}_\mathrm{M}$ is directly proportional to the magnitude of the applied in-plane magnetic field. This results into a transition to a gapless indirect semimetal phase at a critical value of the magnetic field. Therefore, already at quite small magnetic field there is no bulk gap protecting the edge states.

Moreover, the top (bottom) of the hole (electron) band shifts upwards (downwards). This results in a lopsided looking edge spectrum, where a direct gap in absence of magnetic field becomes an indirect gap as the magnetic field is increased. At some critical value of the magnetic field, the electron and hole band overlap. Even so, there is no bulk-gap that is protecting these "edge" states. The consideration of interaction effects may explain this behaviour.

Zeeman Effect: Zeeman field breaks the time-reversal symmetry and opens a gap in the edge state spectrum. However, this effect is much weaker than the orbital effect which leads to bulk gap closing.

Role of disorder: If an on-site impurity potential is added in the presence of in-plane magnetic field, the quantized edge conductance is only weakly destroyed and localized states with relatively long localization length may appear [146, 149].

In this chapter, we looked into the main differences between a type-I and type-II quantum wells. The lower value of the tunneling term A and the bulk-inversion asymmetry term Δ_z in type-II quantum wells, play an important role when Coulomb interactions are included. This will be studied in the next chapter.

Chapter 3

Interplay of excitons and the quantum spin Hall effect

In this chapter, we discuss why including Coulomb interactions in type-II quantum wells, lead to the formation of excitons in these systems. We study the effect of excitons on the topological phase transition. This forms the preliminary study of this system for the original work presented in next chapter.

3.1 Excitons in Type-II quantum well

An electron from a conduction band and a hole from a valence band form a bound state called exciton. The excitons can become a condensate under certain conditions [150, 151]. The Coulomb interactions between the electrons and holes is the main reason behind the formation of this bound state. In addition to optically generated excitons, it has been found that excitons are also created from spatially separated electron and hole layers [152–155] with experimental observations in bilayers [128–131]. The magnitude of the lifetime of excitons which are generated from a bilayer configuration is greater than the excitons created from optical excitations [152]. One of the requirements to obtain an exciton condensate phase in such systems is to have zero to very weak tunneling processes between the electron and hole layers. Therefore, the bilayer configuration in InAs/GaSb quantum wells, where the weakly coupled electron and hole subbands are separated in different materials becomes a good setup to realize excitons [87, 151]. There have been several experimental signatures of the presence of exciton condensate phases in these double quantum well structures [88]. Contrary to type-II quantum wells, it is difficult to obtain an exciton condensate phase in type-I quantum well structures, as the electron and hole subband are strongly coupled [85, 133].

As has been discussed before, it has been observed in experiments that the conductance is quantized for very large values of magnetic field for short samples [70]. In long samples and in the absence of magnetic field, the longitudinal resistance increases linearly with the length of the device [85]. Moreover, the mean free path is found to be temperature independent for a temperature range of 20 mK to 4.2K [70–72]. Interactions and disorder have been considered as possible explanations for the above experimental observations. The temperature independent mean-free path suggest the presence of elastic backscattering effects. These backscattering effects could be a result of a spontaneously or dynamically broken time-reversal symmetry. The order of the observed mean free path suggests that dynamically broken time-reversal symmetry may be unlikely [85].

In Ref. [85], which becomes the motivation behind the publications comprising this thesis, the authors study the presence of Coulomb interactions in type-II quantum well, which is referred to as an electron-hole bilayer in the paper, by performing a mean-field analysis of the total Hamiltonian. The numerical Hartree-Fock mean-field calculations in the presence of the Coulomb interactions lead to a simplified mean-field potential which captures the spin structure of the excitons in the bilayer:

$$\begin{aligned}\Delta^{mf}(\mathbf{k}) \;=\;& \Re[\Delta_1]\tau_y\sigma_y + \Re[\Delta_2](k_x\tau_x\sigma_z - k_y\tau_y\sigma_0)\\ &+\Im[\Delta_1]\tau_x\sigma_y - \Im[\Delta_2](k_x\tau_y\sigma_z + k_y\tau_x\sigma_0),\end{aligned} \tag{3.1}$$

where τ's and σ's are the Pauli matrices that stand for electron-hole and spin degrees of freedom, and Δ_1 and Δ_2 are complex valued, bosonic fields designated for s-wave and p-wave pairing between the excitons. The real and imaginary parts of these pairings have been written separately in (3.1) because the imaginary parts become order parameters for TRS breaking, as shown subsequently. The simplified mean field term (3.1) acts as the interaction term H_{EC} which is added to the single particle Hamiltonian H_0 (2.1), introduced in the previous chapter. As can be seen from (3.1), only interaction between the electron and hole bands are considered. Coulomb interactions within each band are neglected as they only result in renormalisation of the energy bands [85]. As was done in the previous chapter, the k-dependant spin-orbit couplings that arise from bulk and structural inversion asymmetry terms will also not be considered in the main calculations.

In the calculations present henceforth, we will see the effect of excitons that appear as a result of Coulomb interactions between the electron and hole band. As was done in the previous chapter, the natural units for all parameters used in the calculations will be E_0 and d_0, which are the exciton binding energy and the Bohr radius, respectively. The values of these units are determined by equating the Bohr formula for the hydrogen atom with the Coulomb energy [85]:

$$E_0 = \frac{\hbar^2}{2m_{\mathrm{eff}}d_0^2} = \frac{1}{4\pi\epsilon\epsilon_0}\frac{e^2}{d_0} \tag{3.2}$$

3.1.1 Obtaining the exciton pairings

The simplified expression for the mean-field potential, (3.1) is used in the Hartree-Fock mean field equations. This gives the following expressions to obtain the values of Δ_1 and Δ_2 [125]:

$$\begin{aligned} \Delta_1 &= \frac{g_s d_0^2}{(2\pi)^2}\int d^2k\left[\langle c^\dagger_{\mathbf{k}\downarrow 2}c_{\mathbf{k}\uparrow 1}\rangle - \langle c^\dagger_{\mathbf{k}\uparrow 2}c_{\mathbf{k}\downarrow 1}\rangle\right] \\ \Delta_2 &= \frac{g_p d_0^4}{(2\pi)^2}\int\left[-\langle c^\dagger_{\mathbf{k}\uparrow 2}c_{\mathbf{k}\uparrow 1}\rangle(k_x - ik_y) + \langle c^\dagger_{\mathbf{k}\downarrow 2}c_{\mathbf{k}\downarrow 1}\rangle(k_x + ik_y)\right] \end{aligned} \tag{3.3}$$

where g_s and g_p are the s-wave and p-wave pairing strengths of excitons. The electron annihilation operators are $c_{k\sigma 2}$ and $c_{k\sigma 1}$ for the electron and hole bands respectively. Choosing the best values of the interaction strengths g_s and g_p between excitons allows one to get approximately the same results from Hartree-Fock calculations in Ref [85].

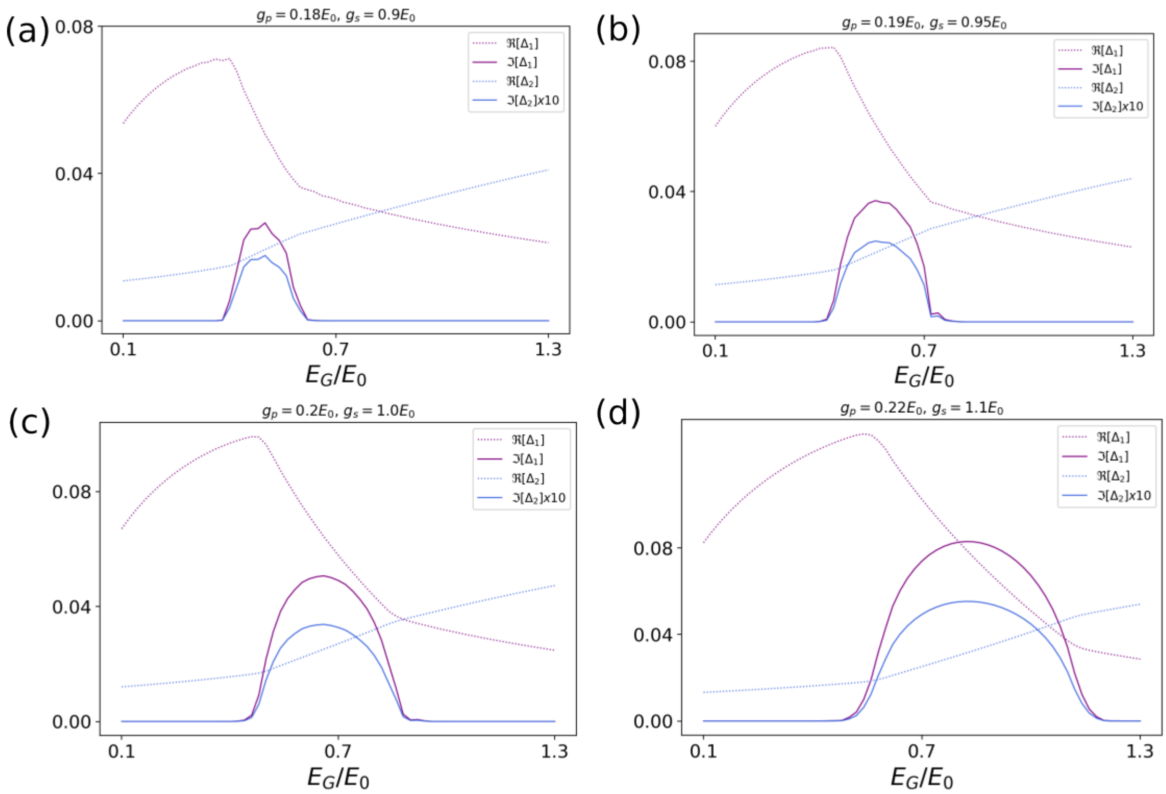

Figure 3.1: Phase diagram as a function of E_G for different fitting parameters. (a) $g_p = 0.18E_0$, $g_s = 0.9E_0$, (b) $g_p = 0.19E_0$, $g_s = 0.95E_0$, (c) $g_p = 0.2E_0$, $g_s = 1.0E_0$ and (d) $g_p = 0.22E_0$, $g_s = 1.1E_0$.

For the choice of $g_s = 1.0E_0$ and $g_p = 0.2E_0$, the time-reversal symmetry breaking order parameters become non-zero for approximately the same range as the Hartree-Fock calculations performed in Ref. [85]. From the phase diagram presented as a function E_G/E_0 for $g_s = 1.0E_0$ and $g_p = 0.2E_0$, we can see that for small values E_G, $\Re[\Delta_1] > \Re[\Delta_2]$ and for large values of E_G, $\Re[\Delta_1] < \Re[\Delta_2]$ while $\Im[\Delta_1, \Delta_2] = 0$ for both cases. Only for intermediate values of E_G are the $\Im[\Delta_1, \Delta_2]$ taking non-zero values (see Fig. 3.1c). In the following sections, all calculations have been performed with the above of choice of fitting parameters.

3.2 Topological Phase transition

The time-reversal symmetry operator is defined as $\mathcal{T} = i\tau_0\sigma_y\mathcal{K}$ where $\mathcal{K}$ is the complex conjugation operator. Let the total Hamiltonian be defined as $H = H_0 + H_{\rm EC}$, the time reversal symmetry operator $\mathcal{T}$ commutes with H, if the imaginary terms $\Im[\Delta_1, \Delta_2] = 0$. This suggests that the imaginary parts of excitonic pairings break time-reversal symmetry. From the previous section, we know that for intermediate values of E_G, there exists a region where $\Im[\Delta_1, \Delta_2] \neq 0$. This is the range of E_G, where the time-reversal symmetry is spontaneously broken [85].

The time reversal symmetry breaking order parameter is defined in the following way:

$$\mathcal{T}^{\rm br} = \frac{\Delta_{\rm tot}^{\rm br}}{\Delta_{\rm tot}^{\rm br} + \Delta_{\rm tot}^{\rm ts}} \tag{3.4}$$

where

$$\begin{aligned}(\Delta_{\rm tot}^{\rm ts})^2 &= \left((\Re[\Delta_2]k_{\rm F})^2 + (\Re[\Delta_1])^2\right) \\ (\Delta_{\rm tot}^{\rm br})^2 &= \left((\Im[\Delta_2]k_{\rm F})^2 + (\Im[\Delta_1])^2\right)\end{aligned} \tag{3.5}$$

where the Fermi momentum $k_{\rm F} = \sqrt{2mE_G}/\hbar$. The terms $\Delta_{\rm tot}^{\rm br}$ and $\Delta_{\rm tot}^{\rm ts}$ denote the relative strength of mean field amplitudes breaking and preserving the time-reversal symmetry respectively. For $A = \Delta_z = 0$, the exciton condensate phase appears in the system. As A and Δ_z is switched on, they act as symmetry breaking terms and turns the exciton condensate phase into a crossover, where correlated phases of excitons exist [85]. As is seen from the phase diagram Fig. 3.2, for small and large values of A and E_G, the $\mathcal{T}^{\mathrm{br}}$ is zero. However, there exists a region of non-zero values of $\mathcal{T}_{\mathrm{br}}$ where the excitons break time-reversal symmetry spontaneously.

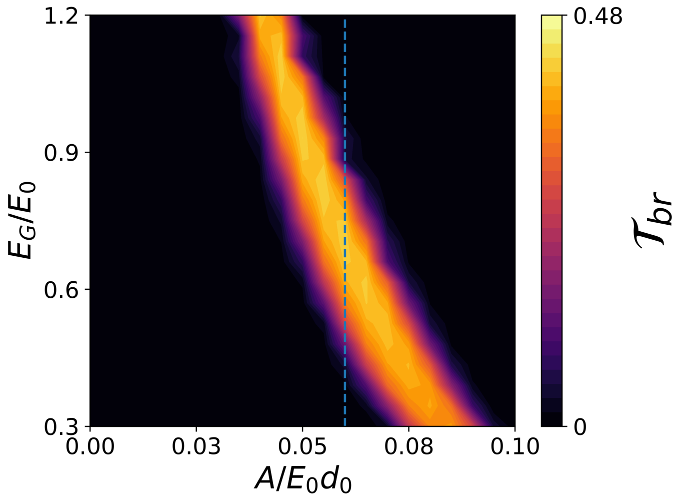

Figure 3.2: Phase diagram of the time-reversal symmetry broken order parameter $\mathcal{T}_{br}$ as a function of E_G/E_0 and A/E_0d_0. The dark (colourful) region denotes the region where time-reversal symmetry is preserved (is spontaneously broken). The value of k_F considers $m = \hbar = 1$, therefore $k_F = \sqrt{2E_G}$.

In order to identify the topological nature of the phases on either side of this time-reversal symmetry broken phase, a parity operator $\mathcal{P}$ is introduced. This is an indicator of the topological phase of the system and is defined as:

$$\mathcal{P} = \frac{\Delta_{\mathrm{tot}}^{\mathrm{even}} - \Delta_{\mathrm{tot}}^{\mathrm{odd}}}{\Delta_{\mathrm{tot}}^{\mathrm{even}} + \Delta_{\mathrm{tot}}^{\mathrm{odd}}} \tag{3.6}$$

where

$$\begin{aligned} (\Delta_{\mathrm{tot}}^{\mathrm{even}})^2 &= |\Delta_1|^2 \\ (\Delta_{\mathrm{tot}}^{\mathrm{odd}})^2 &= (|\Delta_2|k_{\mathrm{F}})^2. \end{aligned} \tag{3.7}$$

Let us now understand why $\Delta_{\mathrm{tot}}^{\mathrm{even}}(\Delta_{\mathrm{tot}}^{\mathrm{odd}})$ is related to $|\Delta_1|(|\Delta_2|)$. When Coulomb interactions are included, the s-wave pairing potential Δ_1 couples with Δ_z term, whereas the p-wave excitonic potential Δ_2 pairs with the A. Therefore, the Δ_1 and Δ_2 terms also have even and odd parity respectively. The parity operator defined in (3.6) is similar to the Z_2 topological invariant introduced in the previous chapter. The understanding of the parity operator $\mathcal{P}$ as the Z_2 topological invariant is only valid when the imaginary parts of the excitonic pairing terms are zero or in other words, the time-reversal symmetry is preserved.

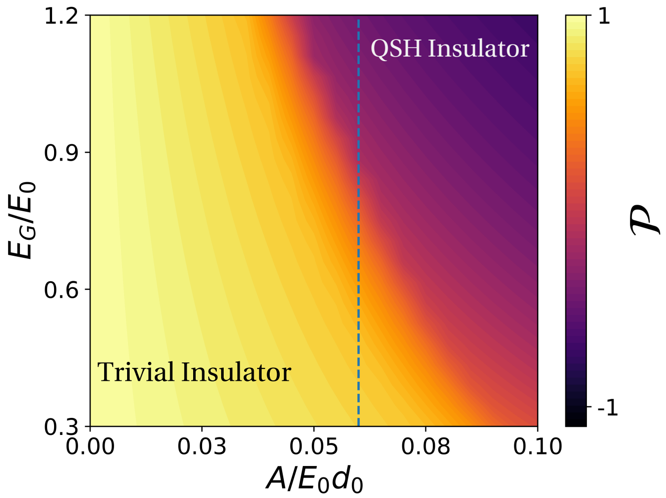

Figure 3.3: Parity of order parameter $\mathcal{P}$ as a function of E_G/E_0 and A/E_0d_0. We notice that for even (odd) parity, the system is in trivial (quantum spin Hall) phase.

For small values of E_G and A, $\Re[\Delta_1] > \Re[\Delta_2]$, this suggests that $\mathcal{P} = 1$ as $\Delta_{\text{tot}}^{\text{even}}$ will dominate in (3.6). On the other hand, for large values of E_G and A, $\mathcal{P} = -1$ because $\Delta_{\text{tot}}^{\text{odd}}$ will dominate the even-parity contribution. The change in the sign of Z_2-like topological invariant for small and large values of E_G and A signifies a change in the topological state.

The phase diagrams of time-reversal symmetry order parameter in Fig. 3.2 and parity order parameter in Fig. 3.3, as a function of E_G/E_0 and A/E_0d_0 are qualitatively similar to phase diagrams presented in Ref. [85]. The simplified mean-field term (3.1), successfully captures the qualitative features of the topological phase transition due to the presence of excitons in Ref. [85]. The energy dispersions for three different values of E_G for an intermediate value of A (denoted by the blue dashed line in Fig. 3.2 and Fig. 3.3) confirms the above analysis. For low value of E_G, the system is in a trivial state and for large values of E_G, the system has helical

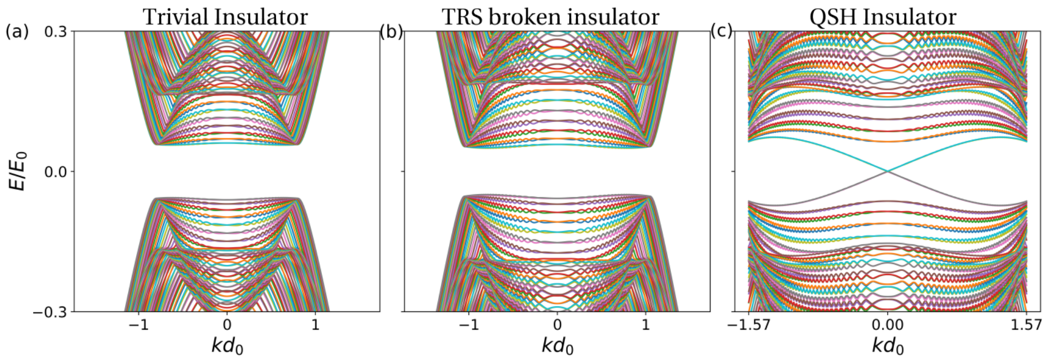

Figure 3.4: Energy bands when the system is a (a) trivial, (b) time-reversal symmetry (TRS) and (c) quantum spin Hall (QSH) insulator. As can be seen, the exciton interactions allow a topological phase transition with no bulk gap closing. The energy spectrums were obtained for $A/E_0d_0 = 0.06$, which is denoted as a blue dashed line in the phase diagrams for time-reversal symmetry and parity order parameters.

edge states which cross the zero energy at Γ point confirming the quantum spin Hall phase. In Ref. [85], the results have also been analysed from the perspective of Ginzburg-Landau theory where the exciton order parameter (3.1) and the tunneling between the two bands act as a perturbation in the free-energy. The first order terms in the expression of free energy are discussed to be proportional to $-\Delta_z\Re[\Delta_1]$ and $-A\Re[\Delta_2]$ and it is energetically favorable to keep the imaginary parts of excitonic pairings to zero. It is the fourth-order terms that try to make the imaginary parts of Δ_1 and Δ_2 non-zero and induce a spontaneous time-reversal symmetry broken phase.

A more intuitive way of understanding this interesting phenomenon is, when $\mathcal{P} = 1$, both A and Δ_2 can be adibatically made zero, the resulting Hamiltonian resembles a BCS s-wave superconductor which does not support edge states and is trivial. Similarly, when $\mathcal{P} = -1$, Δ_z and Δ_1 can be turned off, the system becomes a BHZ Hamiltonian which is a quantum spin Hall insulator with helical edge states. In order to minimise the energy during the topological transition, the system remains gapped and therefore, a spontaneous time-reversal symmtery broken phase appears. Therefore, the consequence of introducing Coulomb interactions in the bilayer is a rich topological phase diagram where the bulk gap does not close.

3.3 Bulk inversion asymmetry term Δ_z

So far, we have understood the role of modulating A and E_G in the bilayer system when Coulomb interactions are allowed. In this section, we will understand the role of Δ_z on the phase diagrams for time-reversal symmetry breaking and parity order parameter.

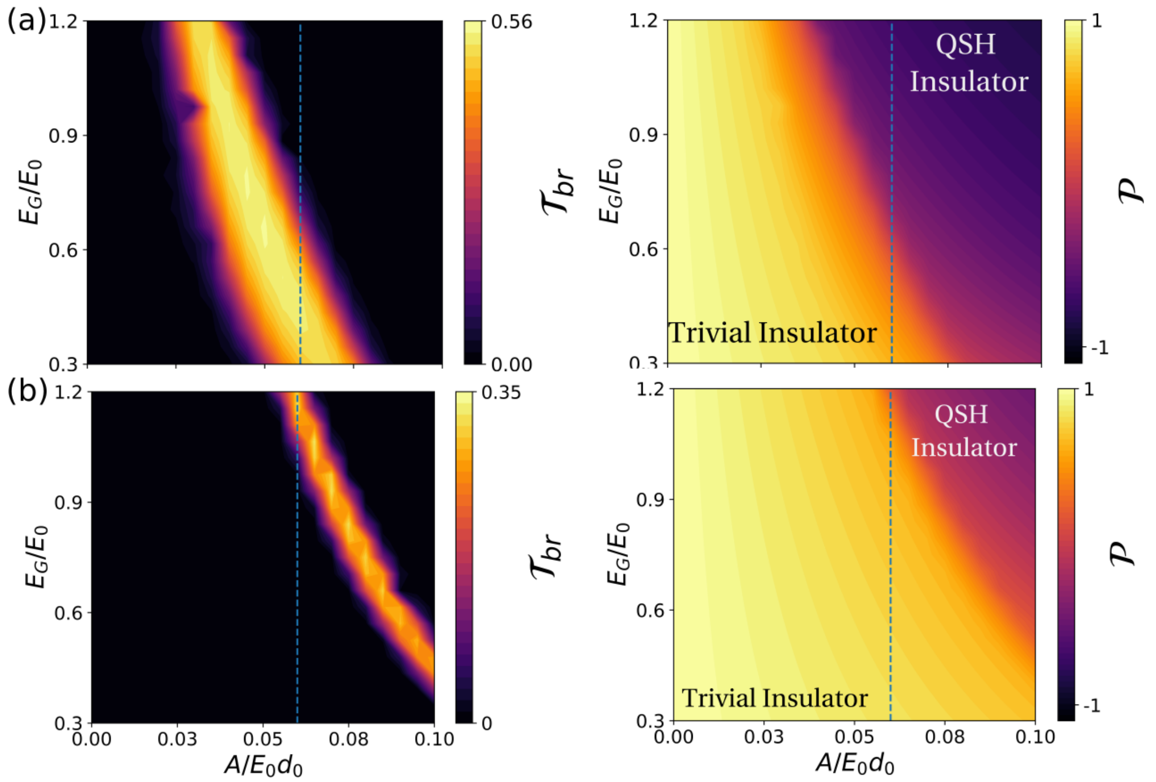

Figure 3.5: Phase diagram of time-reversal symmetry breaking and parity order parameter as a function of E_G/E_0 and A/E_0d_0 for (a) $\Delta_z = 0.01E_0$ and (b) $\Delta_z = 0.04E_0$

Increasing Δ_z has two effects: First, it drives the time-reversal symmetry to break for a larger value of A. The second effect is the reduction of the area of the time-reversal symmetry broken phase as Δ_z increases. As discussed in the previous section, the natural tendency of the system is for the phases of the excitonic pairings to assume zero values. A large magnitude of Δ_z forces the system to minimize the free energy and avoids spontaneously breaking the time-reversal symmetry. This could also explain why the type-I quantum wells do not exhibit an exciton condensate phase as both Δ_z and A are simultaneosly larger compared to type-II quantum wells. Therefore, in order to obtain the TRS broken phase, the value of Δ_z should be much less than $0.1E_0$, since for this value the excitonic pairings is larger than the tunneling amplitude [85].

3.4 Mass asymmetry

So far the effect of interactions were considered when the effective mass of electrons and holes are equal. However, InAs/GaSb display an asymmetry in effective masses of the order $m_e/m_h = 0.84$ [133]. We first check the behaviour of Δ_1 and Δ_2 as function E_G/E_0 and $A/E_0 d_0$, shown as,

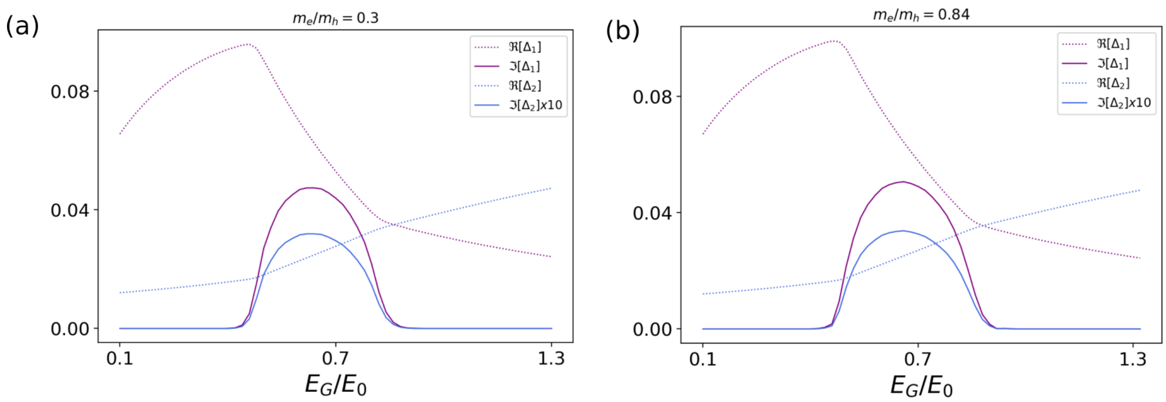

Figure 3.6: Phase diagram as a function of E_G when (a) $m_e/m_h = 0.3$ and (b) $m_e/m_h = 0.84$.

As is visible from the energy phase diagram below, the mass asymmetry does not affect the appearance of the time-reversal symmetry broken phase. Increasing the mass asymmetry by increasing the hole mass, increases the effective mass which raises the critical temperature at which the exciton condensate appears for negligible tunneling term in such bilayers [153].

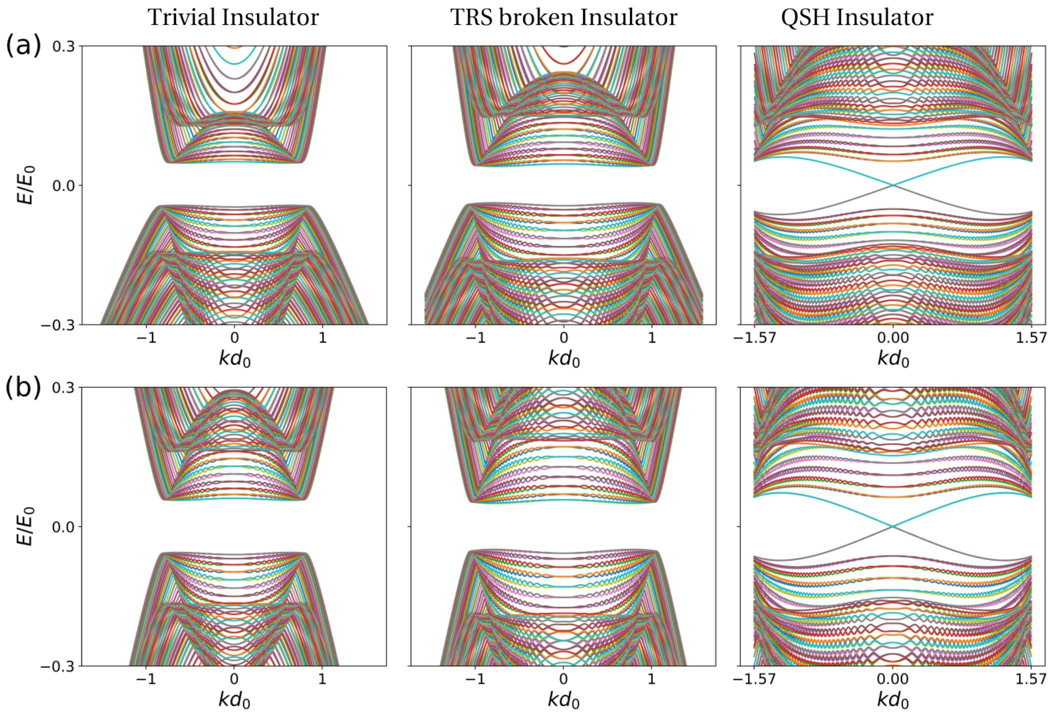

Figure 3.7: Energy bands for different values of E_G/E_0 when (a)$m_e/m_h = 0.3$ and (b)$m_e/m_h = 0.84$

In this chapter, we have looked into how the excitons in type-II quantum wells, lead to an unconventional topological phase transition where there is no bulk-gap closing. Instead, due to the presence of interactions, the system tries to minimise the Free energy, when it is transitioning from trivial to quantum spin Hall phase. This results in a spontaneously broken time-reversal symmetry phase, where the system becomes an insulator.

Chapter 4

Paper I: Interplay of quantum spin Hall effect and spontaneous time-reversal symmetry breaking in electron-hole bilayers I. Transport properties

Summary

The electron-hole bilayer such as InAs/GaSb is a band-inverted system that also supports quantum spin Hall phase as a function of well width and electron-hole densities. However, in experiments, for long samples, this material has shown linearly increasing longitudinal resistance with device length, mean free path of which, is found to be temperature independent for a wide range of temperature of 20mK to 4.2K. An appearance of spontaneously broken time-reversal symmetry phase could allow elastic backscattering processes which may explain the magnitude and temperature independence of the mean free path. As this material is also a candidate for supporting correlated phases of excitons, it has been shown that there is a spontaneous time-reversal symmetry broken phase that appears between trivial and QSH phases in the topological phase diagram as a function of increasing electron-hole densities. The breaking of TRS due to the presence of excitons, leads to an unconventional topological transition where the bulk-gap closing is absent. In the paper below, we present a transport study on a Corbino disc which proposes that this TRS broken phase could be observed in an experiment through measuring bulk and edge conductances as a function of electron-hole densities. As the electron-hole densities are increased, the bulk-conductance remains zero while the edge conductance smoothly takes a quantized value around the Fermi energy, demonstrating the occurrence of a topological transition without bulk-gap closing.

Chapter 5

Paper II: Interplay of quantum spin Hall effect and spontaneous time-reversal symmetry breaking in electron-hole bilayers II. Zero-field Topological Superconductivity

Summary

It has been theoretically proposed that by applying a magnetic field or using ferromagnetic insulators to break TRS in quantum spin Hall insulators in proximity with s-wave superconductors, Majorana zero modes could be realized. The breaking of TRS is necessary to lift the Kramer's degeneracy and obtain well localized Majorana zero modes (MZMs). So far, there has been no successful observation of MZMs from the proposed setup. This is mainly because magnetic field has a detrimental effect on superconductivity and there exists a lack of suitable ferromagnetic insulator materials that can be interfaced with quantum spin Hall insulators. In the paper below, we show that MZMs appear at the interface of a electron-hole bilayer in its TRS broken phase and a superconductor. We calculate a $\mathbb{Z}_2$ topological invariant ν that indicates the parity of the ground state, where the odd (even) value indicates if the system is in topological (trivial) phase. We developed an effective edge theory and analytically show the presence of MZMs at the interface of TRS broken insulator and superconductor. We also propose an experimental setup of superconductor/TRS broken insulator/superconductor Josephson junction, that allows the measurement of the 4π periodic Josephson current, which is one of the experimental signatures of the presence of MZMs. We present an in depth study to find the optimal region of parametric values where the MZMs are experimentally visible. Moreover, a mechanism to demonstrate Majorana fusion-rule is also introduced.

Chapter 6

Conclusion and Outlook

In this thesis, we have looked into the foundational principles of quantum spin Hall effect, which can be understood via analogies to quantum Hall and quantum anomalous Hall effects. We have studied the model by A. Bernevig, T. Hughes and S.C. Zhang which describes the quantum spin Hall effect observed in the band-inverted regime of type-I and type-II quantum wells. We have discussed the significant role of Coulomb interactions because of the spatially separated electron and hole subbands in type-II quantum wells. The Coulomb interactions in these quantum wells lead to the formation of an exciton condensate phase. By varying the tunneling term between the electron and hole layers, it is possible to turn the exciton condensate phase into a crossover. In this regime, it has been shown theoretically, that the correlated excitons lead to spontaneous time-reversal symmetry breaking for intermediate strengths of tunneling and the electron-hole density, which is controlled by the Dirac mass term E_G in the Hamiltonian. This time-reversal symmetry broken phase appears in between the trivial and quantum spin Hall phase. This results in an unconventional topological phase transition where the bulk-gap does not close. In the work comprising the first paper, we found that:

- The proposed experimental setup of a Corbino disc can be used to confirm the presence of an unconventional topological phase transition. We also test the topological phase transition in the presence of varied disorder strengths and mass asymmetry, and find that the transport characteristics confirm the existence of the unconventional topological phase transition in all realistic situations.

We further discussed the possibility of utilizing the time-reversal broken phase that appears in type-II quantum wells due to excitons to realize Majorana zero modes. This avoids the problems that arise in the state of the art setups which use magnetic field or ferromagnetic insulators to break time-reversal symmetry. Our calculations presented in the second paper show that:

- It is possible to realize Majorana zero modes at the interface of a type-II quantum well in its spontaneously broken time-reversal symmetry phase and an s-wave superconductor.
- A superconductor/time-reversal symmetry broken insulator/superconductor Josephson junction provided an experimental signature of the Majorana zero modes that are present.
- Our theoretical prediction could be confirmed in state-of-the-art experimental devices.

In conclusion, we have answered the main three questions that formed the research problem for the doctoral dissertation.
Quantum spin Hall insulators offer quantized conductance only for short samples. Therefore, it is important to consider the role of interactions for a better insight into the physics of such materials. The emergence of correlated phases of excitons in bilayer systems as a result of Coulomb interactions have been studied extensively in theoretical frameworks and are also becoming increasingly evident in the experiments. Therefore, it is important to explore the interaction effects in topological materials, both experimentally and theoretically. Moreover, as has been shown, one could use interactions to realize Majorana zero modes. An experimental observation of these quasiparticles would solve one of the major problems in condensed matter physics.

Bibliography

[1] E. H. Hall. "On a New Action of the Magnet on Electric Currents". In: *American Journal of Mathematics* 2.3 (1879), pp. 287–292. ISSN: 00029327, 10806377.

[2] S. Datta. *Electronic Transport in Mesoscopic Systems*. Cambridge Studies in Semiconductor Physics and Microelectronic Engineering. Cambridge University Press, 1995. DOI: 10.1017/CBO9780511805776.

[3] K. von Klitzing, G. Dorda, and M. Pepper. "New Method for High-Accuracy Determination of the Fine-Structure Constant Based on Quantized Hall Resistance". In: *Phys. Rev. Lett.* 45 (1980), pp. 494–497. DOI: 10.1103/PhysRevLett.45.494.

[4] R. B. Laughlin. "Quantized Hall conductivity in two dimensions". In: *Phys. Rev. B* 23 (1981), pp. 5632–5633. DOI: 10.1103/PhysRevB.23.5632.

[5] B. I. Halperin. "Quantized Hall conductance, current-carrying edge states, and the existence of extended states in a two-dimensional disordered potential". In: *Phys. Rev. B* 25 (1982), pp. 2185–2190. DOI: 10.1103/PhysRevB.25.2185.

[6] J. Weis and K. von Klitzing. "Metrology and microscopic picture of the integer quantum Hall effect". In: *Philosophical Transactions of the Royal Society A: Mathematical, Physical and Engineering Sciences* 369.1953 (2011), pp. 3954–3974. DOI: 10.1098/rsta.2011.0198.

[7] Z. Jiang et al. "Quantum Hall effect in graphene". In: *Solid State Communications* 143.1 (2007). Exploring graphene, pp. 14–19. ISSN: 0038-1098. DOI: 10.1016/j.ssc.2007.02.046.

[8] NobelPrize.org. *The Nobel Prize in Physics 1985*. URL: `https://www.nobelprize.org/prizes/physics/1985/summary/`.

[9] R. B. Laughlin. "Anomalous Quantum Hall Effect: An Incompressible Quantum Fluid with Fractionally Charged Excitations". In: *Phys. Rev. Lett.* 50 (1983), pp. 1395–1398. DOI: `10.1103/PhysRevLett.50.1395`.

[10] H. L. Stormer, D. C. Tsui, and A. C. Gossard. "The fractional quantum Hall effect". In: *Rev. Mod. Phys.* 71 (1999), S298–S305. DOI: `10.1103/RevModPhys.71.S298`.

[11] D. C. Tsui, H. L. Stormer, and A. C. Gossard. "Two-Dimensional Magnetotransport in the Extreme Quantum Limit". In: *Phys. Rev. Lett.* 48 (1982), pp. 1559–1562. DOI: `10.1103/PhysRevLett.48.1559`.

[12] J.P. Eisenstein. "Exciton Condensation in Bilayer Quantum Hall Systems". In: *Annual Review of Condensed Matter Physics* 5.1 (2014), pp. 159–181. DOI: `10.1146/annurev-conmatphys-031113-133832`.

[13] B. Andrei Bernevig, Taylor L. Hughes, and Shou-Cheng Zhang. "Quantum Spin Hall Effect and Topological Phase Transition in HgTe Quantum Wells". In: *Science* 314.5806 (2006), pp. 1757–1761. DOI: `10.1126/science.1133734`.

[14] M. König et al. "Quantum Spin Hall Insulator State in HgTe Quantum Wells". In: *Science* 318.5851 (2007), pp. 766–770. DOI: `10.1126/science.1148047`.

[15] F. D. M. Haldane. "Model for a Quantum Hall Effect without Landau Levels: Condensed-Matter Realization of the "Parity Anomaly" ". In: *Phys. Rev. Lett.* 61 (1988), pp. 2015–2018. DOI: `10.1103/PhysRevLett.61.2015`.

[16] X. L. Qi, Y. S. Wu, and S. C. Zhang. "Topological quantization of the spin Hall effect in two-dimensional paramagnetic semiconductors". In: *Phys. Rev. B* 74 (2006), p. 085308. DOI: `10.1103/PhysRevB.74.085308`.

[17] C. Z. Chang et al. "Experimental Observation of the Quantum Anomalous Hall Effect in a Magnetic Topological Insulator". In: *Science* 340.6129 (2013), pp. 167–170. DOI: `10.1126/science.1234414`.

[18] C. Nayak et al. "Non-Abelian anyons and topological quantum computation". In: *Rev. Mod. Phys.* 80 (2008), pp. 1083–1159. DOI: 10.1103/RevModPhys.80.1083.

[19] S. S. Hegde et al. "Quasinormal Modes and the Hawking-Unruh Effect in Quantum Hall Systems: Lessons from Black Hole Phenomena". In: *Phys. Rev. Lett.* 123 (2019), p. 156802. DOI: 10.1103/PhysRevLett.123.156802.

[20] S. C. Zhang and J. Hu. "A Four-Dimensional Generalization of the Quantum Hall Effect". In: *Science* 294.5543 (2001), pp. 823–828. DOI: 10.1126/science.294.5543.823.

[21] L. D. Landau and L. M. Lifshitz. *Quantum Mechanics Non-Relativistic Theory, Third Edition: Volume 3*. Butterworth-Heinemann, 1981.

[22] David Tong. *Lectures on the Quantum Hall Effect*. 2016. DOI: 10.48550/arXiv.1606.06687.

[23] F. Delahaye and B. Jeckelmann. "Revised technical guidelines for reliable dc measurements of the quantized Hall resistance". In: *Metrologia* 40.5 (2003), p. 217. DOI: 10.1088/0026-1394/40/5/302.

[24] A. Fabre et al. "Laughlin's Topological Charge Pump in an Atomic Hall Cylinder". In: *Phys. Rev. Lett.* 128 (2022), p. 173202. DOI: 10.1103/PhysRevLett.128.173202.

[25] K. von Klitzing et al. "40 years of the quantum Hall effect". In: *Nature Reviews Physics* 2.8 (2020), pp. 397–401. DOI: 10.1038/s42254-020-0209-1.

[26] D. J. Thouless et al. "Quantized Hall Conductance in a Two-Dimensional Periodic Potential". In: *Phys. Rev. Lett.* 49 (1982), pp. 405–408. DOI: 10.1103/PhysRevLett.49.405.

[27] Charles Kittel. *Introduction to Solid State Physics*. 8th ed. Wiley, 2004. ISBN: 9780471415268.

[28] N. W. Ashcroft and N. D. Mermin. *Solid State Physics*. Holt-Saunders, 1976.

[29] M. Kohmoto. "Topological invariant and the quantization of the Hall conductance". In: *Annals of Physics* 160.2 (1985), pp. 343–354. DOI: `10.1016/0003-4916(85)90148-4`.

[30] B. Simon. "Holonomy, the Quantum Adiabatic Theorem, and Berry's Phase". In: *Phys. Rev. Lett.* 51 (1983), pp. 2167–2170. DOI: `10.1103/PhysRevLett.51.2167`.

[31] M. Berry. "Quantal phase factors accompanying adiabatic changes". In: *Proceedings of the Royal Society of London. A. Mathematical and Physical Sciences* 392.1802 (1984), pp. 45–57. DOI: `10.1098/rspa.1984.0023`.

[32] M. Berry. "Anticipations of the Geometric Phase". In: *Physics Today* 43.12 (1990), pp. 34–40. DOI: `10.1063/1.881219`.

[33] D. B. Chklovskii, B. I. Shklovskii, and L. I. Glazman. "Electrostatics of edge channels". In: *Phys. Rev. B* 46 (1992), pp. 4026–4034. DOI: `10.1103/PhysRevB.46.4026`.

[34] M. Büttiker. "Absence of backscattering in the quantum Hall effect in multiprobe conductors". In: *Phys. Rev. B* 38 (1988), pp. 9375–9389. DOI: `10.1103/PhysRevB.38.9375`.

[35] M. Z. Hasan and C. L. Kane. "Colloquium: Topological insulators". In: *Rev. Mod. Phys.* 82 (2010), pp. 3045–3067. DOI: `10.1103/RevModPhys.82.3045`.

[36] B.A. Bernevig. *Topological Insulators and Topological Superconductors*. Princeton: Princeton University Press, 2013. ISBN: 9781400846733. DOI: `10.1515/9781400846733`.

[37] J. K. Asbóth, L. Oroszlány, and A. Pályi. *A Short Course on Topological Insulators*. Springer International Publishing, 2016. DOI: `10.1007/978-3-319-25607-8`.

[38] H. Yasuhiro. "Chern number and edge states in the integer quantum Hall effect". In: *Phys. Rev. Lett.* 71 (1993), pp. 3697–3700. DOI: `10.1103/PhysRevLett.71.3697`.

[39] NobelPrize.org. *The Nobel Prize in Physics 1998*. URL: https://www.nobelprize.org/prizes/physics/1998/summary/.

[40] M. B. Hastings and X. G. Wen. “Quasiadiabatic continuation of quantum states: The stability of topological ground-state degeneracy and emergent gauge invariance”. In: *Phys. Rev. B* 72 (2005), p. 045141. DOI: 10.1103/PhysRevB.72.045141.

[41] M. B. Hastings and S. Michalakis. “Quantization of Hall Conductance for Interacting Electrons on a Torus”. In: *Communications in Mathematical Physics* 334.1 (2015), pp. 433–471. DOI: 10.1007/s00220-014-2167-x.

[42] B. I. Halperin. “Possible States for a Three-Dimensional Electron Gas in a Strong Magnetic Field”. In: *Japanese Journal of Applied Physics* 26.S3-3 (1987), p. 1913. DOI: 10.7567/JJAPS.26S3.1913.

[43] M. Kohmoto, B. I. Halperin, and Y. S. Wu. “Diophantine equation for the three-dimensional quantum Hall effect”. In: *Phys. Rev. B* 45 (1992), pp. 13488–13493. DOI: 10.1103/PhysRevB.45.13488.

[44] J. Gooth, S. Galeski, and T. Meng. “Quantum-Hall physics and three dimensions”. In: *Reports on Progress in Physics* 86.4 (2023), p. 044501. DOI: 10.1088/1361-6633/acb8c9.

[45] K. S. Novoselov et al. “Room-Temperature Quantum Hall Effect in Graphene”. In: *Science* 315.5817 (2007), pp. 1379–1379. DOI: 10.1126/science.1137201.

[46] C. X. Liu, S. C. Zhang, and X. L. Qi. “The Quantum Anomalous Hall Effect: Theory and Experiment”. In: *Annual Review of Condensed Matter Physics* 7.1 (2016), pp. 301–321. DOI: 10.1146/annurev-conmatphys-031115-011417.

[47] H. Chi and J. S. Moodera. “Progress and prospects in the quantum anomalous Hall effect”. In: *APL Materials* 10.9 (2022), p. 090903. DOI: 10.1063/5.0100989.

[48] C. Z. Chang, C. X. Liu, and A. H. MacDonald. “Colloquium: Quantum anomalous Hall effect”. In: *Rev. Mod. Phys.* 95 (2023), p. 011002. DOI: 10.1103/RevModPhys.95.011002.

[49] J. Gregor et al. “Experimental realization of the topological Haldane model with ultracold fermions”. In: *Nature* 515.7526 (2014), pp. 237–240. DOI: 10.1038/nature13915.

[50] A. L. Sharpe et al. “Emergent ferromagnetism near three-quarters filling in twisted bilayer graphene”. In: *Science* 365.6453 (2019), pp. 605–608. DOI: 10.1126/science.aaw3780.

[51] M. Serlin et al. “Intrinsic quantized anomalous Hall effect in a moiré heterostructure”. In: *Science* 367.6480 (2020), pp. 900–903. DOI: 10.1126/science.aay5533.

[52] T. Li et al. “Quantum anomalous Hall effect from intertwined moiré bands”. In: *Nature* 600.7890 (2021), pp. 641–646. DOI: 10.1038/s41586-021-04171-1.

[53] Y. Deng et al. “Quantum anomalous Hall effect in intrinsic magnetic topological insulator $MnBi_2Te_4$”. In: *Science* 367.6480 (2020), pp. 895–900. DOI: 10.1126/science.aax8156.

[54] E. J. Fox et al. “Part-per-million quantization and current-induced breakdown of the quantum anomalous Hall effect”. In: *Phys. Rev. B* 98 (2018), p. 075145. DOI: 10.1103/PhysRevB.98.075145.

[55] M. Götz et al. “Precision measurement of the quantized anomalous Hall resistance at zero magnetic field”. In: *Applied Physics Letters* 112.7 (2018). 072102. DOI: 10.1063/1.5009718.

[56] Yi-Fan Zhao et al. “Tuning the Chern number in quantum anomalous Hall insulators”. In: *Nature* 588.7838 (2020), pp. 419–423. DOI: 10.1038/s41586-020-3020-3.

[57] B. A. Bernevig and S. C. Zhang. “Quantum Spin Hall Effect”. In: *Phys. Rev. Lett.* 96 (2006), p. 106802. DOI: 10.1103/PhysRevLett.96.106802.

[58] M. Z. Hasan and C. L. Kane. “Colloquium: Topological insulators”. In: *Rev. Mod. Phys.* 82 (2010), pp. 3045–3067. DOI: 10.1103/RevModPhys.82.3045.

[59] X. L. Qi and S. C. Zhang. "Topological insulators and superconductors". In: *Rev. Mod. Phys.* 83 (2011), pp. 1057–1110. DOI: 10.1103/RevModPhys.83.1057.

[60] C. X. Liu et al. "Quantum Spin Hall Effect in Inverted Type-II Semiconductors". In: *Phys. Rev. Lett.* 100 (2008), p. 236601. DOI: 10.1103/PhysRevLett.100.236601.

[61] M. König et al. "The Quantum Spin Hall Effect: Theory and Experiment". In: *Journal of the Physical Society of Japan* 77.3 (2008), p. 031007. DOI: 10.1143/JPSJ.77.031007.

[62] J. Maciejko, X. L. Qi, and S. C. Zhang. "Magnetoconductance of the quantum spin Hall state". In: *Phys. Rev. B* 82 (2010), p. 155310. DOI: 10.1103/PhysRevB.82.155310.

[63] C. L. Kane and E. J. Mele. "Quantum Spin Hall Effect in Graphene". In: *Phys. Rev. Lett.* 95 (2005), p. 226801. DOI: 10.1103/PhysRevLett.95.226801.

[64] C. L. Kane and E. J. Mele. "Z_2 Topological Order and the Quantum Spin Hall Effect". In: *Phys. Rev. Lett.* 95 (2005), p. 146802. DOI: 10.1103/PhysRevLett.95.146802.

[65] Y. Yao et al. "Spin-orbit gap of graphene: First-principles calculations". In: *Phys. Rev. B* 75 (2007), p. 041401. DOI: 10.1103/PhysRevB.75.041401.

[66] H. Min et al. "Intrinsic and Rashba spin-orbit interactions in graphene sheets". In: *Phys. Rev. B* 74 (2006), p. 165310. DOI: 10.1103/PhysRevB.74.165310.

[67] C. Wu, B. A. Bernevig, and S. C. Zhang. "Helical Liquid and the Edge of Quantum Spin Hall Systems". In: *Phys. Rev. Lett.* 96 (2006), p. 106401. DOI: 10.1103/PhysRevLett.96.106401.

[68] C. Xu and J. E. Moore. "Stability of the quantum spin Hall effect: Effects of interactions, disorder, and $\mathbb{Z}_2$ topology". In: *Phys. Rev. B* 73 (2006), p. 045322. DOI: 10.1103/PhysRevB.73.045322.

[69] A. Altland and M. R. Zirnbauer. “Nonstandard symmetry classes in mesoscopic normal-superconducting hybrid structures”. In: *Phys. Rev. B* 55 (1997), pp. 1142–1161. DOI: 10.1103/PhysRevB.55.1142.

[70] L. Du et al. “Robust Helical Edge Transport in Gated InAs/GaSb Bilayers”. In: *Phys. Rev. Lett.* 114 (2015), p. 096802. DOI: 10.1103/PhysRevLett.114.096802.

[71] I. Knez et al. “Observation of Edge Transport in the Disordered Regime of Topologically Insulating InAs/GaSb Quantum Wells”. In: *Phys. Rev. Lett.* 112 (2014), p. 026602. DOI: 10.1103/PhysRevLett.112.026602.

[72] E. M. Spanton et al. “Images of Edge Current in InAs/GaSb Quantum Wells”. In: *Phys. Rev. Lett.* 113 (2014), p. 026804. DOI: 10.1103/PhysRevLett.113.026804.

[73] A. Roth et al. “Nonlocal Transport in the Quantum Spin Hall State”. In: *Science* 325.5938 (2009), pp. 294–297. DOI: 10.1126/science.1174736.

[74] K. C. Nowack et al. “Imaging currents in HgTe quantum wells in the quantum spin Hall regime”. In: *Nature Materials* 12.9 (2013), pp. 787–791. DOI: 10.1038/nmat3682.

[75] K. Suzuki et al. “Edge channel transport in the InAs/GaSb topological insulating phase”. In: *Phys. Rev. B* 87 (2013), p. 235311. DOI: 10.1103/PhysRevB.87.235311.

[76] G. Grabecki et al. “Nonlocal resistance and its fluctuations in microstructures of band-inverted HgTe/(Hg,Cd)Te quantum wells”. In: *Phys. Rev. B* 88 (2013), p. 165309. DOI: 10.1103/PhysRevB.88.165309.

[77] I. Knez, R. R. Du, and G. Sullivan. “Evidence for Helical Edge Modes in Inverted InAs/GaSb Quantum Wells”. In: *Phys. Rev. Lett.* 107 (2011), p. 136603. DOI: 10.1103/PhysRevLett.107.136603.

[78] B. L. Altshuler, I. L. Aleiner, and V. I. Yudson. “Localization at the Edge of a 2D Topological Insulator by Kondo Impurities with Random Anisotropies”. In: *Phys. Rev. Lett.* 111 (2013), p. 086401. DOI: 10.1103/PhysRevLett.111.086401.

[79] V. Cheianov and L. I. Glazman. “Mesoscopic Fluctuations of Conductance of a Helical Edge Contaminated by Magnetic Impurities”. In: *Phys. Rev. Lett.* 110 (2013), p. 206803. DOI: 10.1103/PhysRevLett.110.206803.

[80] F. Crépin et al. “Renormalization group approach for the scattering off a single Rashba impurity in a helical liquid”. In: *Phys. Rev. B* 86 (2012), p. 121106. DOI: 10.1103/PhysRevB.86.121106.

[81] T. L. Schmidt et al. “Inelastic Electron Backscattering in a Generic Helical Edge Channel”. In: *Phys. Rev. Lett.* 108 (2012), p. 156402. DOI: 10.1103/PhysRevLett.108.156402.

[82] N. Lezmy, Y. Oreg, and M. Berkooz. “Single and multiparticle scattering in helical liquid with an impurity”. In: *Phys. Rev. B* 85 (2012), p. 235304. DOI: 10.1103/PhysRevB.85.235304.

[83] J. I. Väyrynen, Moshe Goldstein, and Leonid I. Glazman. “Helical Edge Resistance Introduced by Charge Puddles”. In: *Phys. Rev. Lett.* 110 (2013), p. 216402. DOI: 10.1103/PhysRevLett.110.216402.

[84] J. I. Väyrynen et al. “Resistance of helical edges formed in a semiconductor heterostructure”. In: *Phys. Rev. B* 90 (2014), p. 115309. DOI: 10.1103/PhysRevB.90.115309.

[85] D. I. Pikulin and T. Hyart. “Interplay of Exciton Condensation and the Quantum Spin Hall Effect in $\mathrm{InAs/GaSb}$ Bilayers”. In: *Phys. Rev. Lett.* 112 (2014), p. 176403. DOI: 10.1103/PhysRevLett.112.176403.

[86] R. Skolasinski et al. “Robust helical edge transport in quantum spin Hall quantum wells”. In: *Phys. Rev. B* 98 (2018), p. 201404. DOI: 10.1103/PhysRevB.98.201404.

[87] Y. Naveh and B. Laikhtman. “Excitonic Instability and Electric-Field-Induced Phase Transition Towards a Two-Dimensional Exciton Condensate”. In: *Phys. Rev. Lett.* 77 (1996), pp. 900–903. DOI: 10.1103/PhysRevLett.77.900.

[88] L. Du et al. “Evidence for a topological excitonic insulator in InAs/GaSb bilayers”. In: *Nature Communications* 8.1 (2017), p. 1971. DOI: 10.1038/s41467-017-01988-1.

[89] X. Wu et al. “Resistive signature of excitonic coupling in an electron-hole double layer with a middle barrier”. In: *Phys. Rev. B* 99 (2019), p. 085307. DOI: 10.1103/PhysRevB.99.085307.

[90] X. J. Wu et al. “Electrically tuning many-body states in a Coulomb-coupled InAs/InGaSb double layer”. In: *Phys. Rev. B* 100 (2019), p. 165309. DOI: 10.1103/PhysRevB.100.165309.

[91] D. Xiao et al. “Anomalous Quantum Oscillations of Interacting Electron-Hole Gases in Inverted Type-II $\mathrm{InAs/GaSb}$ Quantum Wells”. In: *Phys. Rev. Lett.* 122 (2019), p. 186802. DOI: 10.1103/PhysRevLett.122.186802.

[92] R. Wang et al. “Excitonic topological order in imbalanced electron–hole bilayers”. In: *Nature* 619.7968 (2023), pp. 57–62. DOI: 10.1038/s41586-023-06065-w.

[93] Y. Jia et al. “Evidence for a monolayer excitonic insulator”. In: *Nature Physics* 18.1 (2022), pp. 87–93. DOI: 10.1038/s41567-021-01422-w.

[94] B. Sun et al. “Evidence for equilibrium exciton condensation in monolayer WTe2”. In: *Nature Physics* 18.1 (2022), pp. 94–99. DOI: 10.1038/s41567-021-01427-5.

[95] Y. Q. Wang, M. Papaj, and J. E. Moore. “Breakdown of helical edge state topologically protected conductance in time-reversal-breaking excitonic insulators”. In: (2023). DOI: 10.48550/arXiv.2305.09202.

[96] J. C. Budich, B. Trauzettel, and P. Michetti. “Time Reversal Symmetric Topological Exciton Condensate in Bilayer HgTe Quantum Wells”. In: *Phys. Rev. Lett.* 112 (2014), p. 146405. DOI: 10.1103/PhysRevLett.112.146405.

[97] S. D. Sarma, M. Freedman, and C. Nayak. “Majorana zero modes and topological quantum computation”. In: *npj Quantum Information* 1.1 (2015), p. 15001. DOI: 10.1038/npjqi.2015.1.

[98] J. Alicea. “New directions in the pursuit of Majorana fermions in solid state systems”. In: *Reports on Progress in Physics* 75.7 (2012), p. 076501. DOI: 10.1088/0034-4885/75/7/076501.

[99] M. Leijnse and K. Flensberg. “Introduction to topological superconductivity and Majorana fermions”. In: *Semiconductor Science and Technology* 27.12 (2012), p. 124003. DOI: 10.1088/0268-1242/27/12/124003.

[100] K. Flensberg, F. von Oppen, and A. Stern. “Engineered platforms for topological superconductivity and Majorana zero modes”. In: *Nature Reviews Materials* 6.10 (2021), pp. 944–958. DOI: 10.1038/s41578-021-00336-6.

[101] C.W.J. Beenakker. “Search for Majorana Fermions in Superconductors”. In: *Annual Review of Condensed Matter Physics* 4.1 (2013), pp. 113–136. DOI: 10.1146/annurev-conmatphys-030212-184337.

[102] C. Nayak et al. “Non-Abelian anyons and topological quantum computation”. In: *Rev. Mod. Phys.* 80 (2008), pp. 1083–1159. DOI: 10.1103/RevModPhys.80.1083.

[103] C. W. J. Beenakker. “Search for non-Abelian Majorana braiding statistics in superconductors”. In: *SciPost Phys. Lect. Notes* (2020), p. 15. DOI: 10.21468/SciPostPhysLectNotes.15.

[104] E. Majorana. “Teoria simmetrica dell’elettrone e del positrone”. In: *Il Nuovo Cimento (1924-1942)* 14.4 (1937), pp. 171–184. DOI: 10.1007/BF02961314.

[105] M. M. Salomaa and G. E. Volovik. “Half-Quantum Vortices in Superfluid $^3\mathrm{He}$-A”. In: *Phys. Rev. Lett.* 55 (1985), pp. 1184–1187. DOI: 10.1103/PhysRevLett.55.1184.

[106] A. P. Mackenzie and Y. Maeno. “The superconductivity of $\mathrm{Sr_2RuO_4}$ and the physics of spin-triplet pairing”. In: *Rev. Mod. Phys.* 75 (2003), pp. 657–712. DOI: 10.1103/RevModPhys.75.657.

[107] A Yu Kitaev. "Unpaired Majorana fermions in quantum wires". In: *Physics-Uspekhi* 44.10S (2001), p. 131. DOI: 10.1070/1063-7869/44/10S/S29.

[108] L. Fu and C. L. Kane. "Superconducting Proximity Effect and Majorana Fermions at the Surface of a Topological Insulator". In: *Phys. Rev. Lett.* 100 (2008), p. 096407. DOI: 10.1103/PhysRevLett.100.096407.

[109] J. D. Sau et al. "Generic New Platform for Topological Quantum Computation Using Semiconductor Heterostructures". In: *Phys. Rev. Lett.* 104 (2010), p. 040502. DOI: 10.1103/PhysRevLett.104.040502.

[110] J. Alicea. "Majorana fermions in a tunable semiconductor device". In: *Phys. Rev. B* 81 (2010), p. 125318. DOI: 10.1103/PhysRevB.81.125318.

[111] K. T. Law, P. A. Lee, and T. K. Ng. "Majorana Fermion Induced Resonant Andreev Reflection". In: *Phys. Rev. Lett.* 103 (2009), p. 237001. DOI: 10.1103/PhysRevLett.103.237001.

[112] S. Mi et al. "Proposal for the detection and braiding of Majorana fermions in a quantum spin Hall insulator". In: *Phys. Rev. B* 87 (2013), p. 241405. DOI: 10.1103/PhysRevB.87.241405.

[113] L. Fu and C. L. Kane. "Josephson current and noise at a superconductor/quantum-spin-Hall-insulator/supercon-ductor junction". In: *Phys. Rev. B* 79 (2009), p. 161408. DOI: 10.1103/PhysRevB.79.161408.

[114] C. W. J. Beenakker et al. "Fermion-Parity Anomaly of the Critical Supercurrent in the Quantum Spin-Hall Effect". In: *Phys. Rev. Lett.* 110 (2013), p. 017003. DOI: 10.1103/PhysRevLett.110.017003.

[115] V. S. Pribiag et al. "Edge-mode superconductivity in a two-dimensional topological insulator". In: *Nature Nanotechnology* 10.7 (2015), pp. 593–597. DOI: 10.1038/nnano.2015.86.

[116] J. B. Fu et al. "Experimental review on Majorana zero-modes in hybrid nanowires". In: *Science China Physics, Mechanics & Astronomy* 64.10 (2021), p. 107001. DOI: 10.1007/s11433-021-1737-4.

[117] H. Zhang et al. “RETRACTED ARTICLE: Quantized Majorana conductance”. In: *Nature* 556.7699 (2018), pp. 74–79. DOI: 10.1038/nature26142.

[118] Qing L. H. et al. “RETRACTED: Chiral Majorana fermion modes in a quantum anomalous Hall insulator-superconductor structure”. In: *Science* 357.6348 (2017), pp. 294–299. DOI: 10.1126/science.aag2792.

[119] S. Hart et al. “Induced superconductivity in the quantum spin Hall edge”. In: *Nature Physics* 10.9 (2014), pp. 638–643. DOI: 10.1038/nphys3036.

[120] I. Knez, R. R. Du, and G. Sullivan. “Andreev Reflection of Helical Edge Modes in $\mathrm{InAs}/\mathrm{GaSb}$ Quantum Spin Hall Insulator”. In: *Phys. Rev. Lett.* 109 (2012), p. 186603. DOI: 10.1103/PhysRevLett.109.186603.

[121] R. S. Deacon et al. “Josephson Radiation from Gapless Andreev Bound States in HgTe-Based Topological Junctions”. In: *Phys. Rev. X* 7 (2017), p. 021011. DOI: 10.1103/PhysRevX.7.021011.

[122] S. Vaitiekėnas et al. “Zero-bias peaks at zero magnetic field in ferromagnetic hybrid nanowires”. In: *Nature Physics* 17.1 (2021), pp. 43–47. DOI: 10.1038/s41567-020-1017-3.

[123] B. Jäck, Yonglong Xie, and Ali Yazdani. “Detecting and distinguishing Majorana zero modes with the scanning tunnelling microscope”. In: *Nature Reviews Physics* 3.8 (2021), pp. 541–554. DOI: 10.1038/s42254-021-00328-z.

[124] C.W. Groth et al. “Kwant: a software package for quantum transport”. In: *New Journal of Physics* 16.6 (2014), p. 063065. DOI: 10.1088/1367-2630/16/6/063065.

[125] T. Paul, V. F. Becerra, and T. Hyart. “Interplay of quantum spin Hall effect and spontaneous time-reversal symmetry breaking in electron-hole bilayers. I. Transport properties”. In: *Phys. Rev. B* 106 (2022), p. 235420. DOI: 10.1103/PhysRevB.106.235420.

[126] Yuli V. Nazarov and Yaroslav M. Blanter. *Quantum Transport: Introduction to Nanoscience*. Cambridge University Press, 2009.

[127] G. E. Blonder, M. Tinkham, and T. M. Klapwijk. “Transition from metallic to tunneling regimes in superconducting microconstrictions: Excess current, charge imbalance, and supercurrent conversion”. In: *Phys. Rev. B* 25 (1982), pp. 4515–4532. DOI: 10.1103/PhysRevB.25.4515.

[128] J. P. Eisenstein and A. H. MacDonald. “Bose–Einstein condensation of excitons in bilayer electron systems”. In: *Nature* 432.7018 (2004), pp. 691–694. DOI: 10.1038/nature03081.

[129] I. B. Spielman et al. “Resonantly Enhanced Tunneling in a Double Layer Quantum Hall Ferromagnet”. In: *Phys. Rev. Lett.* 84 (2000), pp. 5808–5811. DOI: 10.1103/PhysRevLett.84.5808.

[130] A. D. K. Finck et al. “Exciton Transport and Andreev Reflection in a Bilayer Quantum Hall System”. In: *Phys. Rev. Lett.* 106 (2011), p. 236807. DOI: 10.1103/PhysRevLett.106.236807.

[131] G. W. Burg et al. “Strongly Enhanced Tunneling at Total Charge Neutrality in Double-Bilayer Graphene-$\mathrm{WSe_2}$ Heterostructures”. In: *Phys. Rev. Lett.* 120 (2018), p. 177702. DOI: 10.1103/PhysRevLett.120.177702.

[132] M. König et al. “Spatially Resolved Study of Backscattering in the Quantum Spin Hall State”. In: *Phys. Rev. X* 3 (2013), p. 021003. DOI: 10.1103/PhysRevX.3.021003.

[133] C. Liu and S. C. Zhang. *Models and Materials for Topological Insulators, edited by M. Franz and L. Molenkamp, Topological Insulators*. Springer, 2013.

[134] L. J. Cooper et al. “Resistance resonance induced by electron-hole hybridization in a strongly coupled InAs/GaSb/AlSb heterostructure”. In: *Phys. Rev. B* 57 (1998), pp. 11915–11918. DOI: 10.1103/PhysRevB.57.11915.

[135] Y. Naveh and B. Laikhtman. “Band-structure tailoring by electric field in a weakly coupled electron-hole system”. In: *Applied Physics Letters* 66.15 (1995), pp. 1980–1982. DOI: 10.1063/1.113297.

[136] V. Lechner. “Bulk and structure inversion asymmetry in semiconductor quantum well structures”. PhD thesis. University of Regensburg, 2012. DOI: 10.5283/epub.25885.

[137] T. Paul, V. F. Becerra, and T. Hyart. “Interplay of quantum spin Hall effect and spontaneous time-reversal symmetry breaking in electron-hole bilayers. II. Zero-field topological superconductivity”. In: *Phys. Rev. B* 106 (2022), p. 235421. DOI: 10.1103/PhysRevB.106.235421.

[138] J. Maciejko, T. L. Hughes, and S. C. Zhang. “The Quantum Spin Hall Effect”. In: *Annual Review of Condensed Matter Physics* 2.1 (2011), pp. 31–53. DOI: 10.1146/annurev-conmatphys-062910-140538.

[139] R. B. Laughlin. “Quantized Hall conductivity in two dimensions”. In: *Phys. Rev. B* 23 (1981), pp. 5632–5633. DOI: 10.1103/PhysRevB.23.5632.

[140] G. Tkachov and E.M. Hankiewicz. “Two-dimensional topological insulators in quantizing magnetic fields”. In: *Physica E: Low-dimensional Systems and Nanostructures* 44.5 (2012), pp. 900–905. DOI: 10.1016/j.physe.2011.11.012.

[141] G. Tkachov and E. M. Hankiewicz. “Ballistic Quantum Spin Hall State and Enhanced Edge Backscattering in Strong Magnetic Fields”. In: *Phys. Rev. Lett.* 104 (2010), p. 166803. DOI: 10.1103/PhysRevLett.104.166803.

[142] J. C. Chen, J. Wang, and Q. F. Sun. “Effect of magnetic field on electron transport in HgTe/CdTe quantum wells: Numerical analysis”. In: *Phys. Rev. B* 85 (2012), p. 125401. DOI: 10.1103/PhysRevB.85.125401.

[143] B. Scharf, A. Matos-Abiague, and J. Fabian. “Magnetic properties of HgTe quantum wells”. In: *Phys. Rev. B* 86 (2012), p. 075418. DOI: 10.1103/PhysRevB.86.075418.

[144] J. R. Meyer et al. “Magneto-optical properties of HgTe-CdTe superlattices”. In: *Phys. Rev. B* 42 (1990), pp. 9050–9062. DOI: 10.1103/PhysRevB.42.9050.

[145] M. Schultz et al. “Crossing of conduction- and valence-subband Landau levels in an inverted HgTe/CdTe quantum well”. In: *Phys. Rev. B* 57 (1998), pp. 14772–14775. DOI: 10.1103/PhysRevB.57.14772.

[146] D. I. Pikulin et al. “Disorder and magnetic-field-induced breakdown of helical edge conduction in an inverted electron-hole bilayer”. In: *Phys. Rev. B* 89 (2014), p. 161403. DOI: 10.1103/PhysRevB.89.161403.

[147] C. W. Groth et al. “Theory of the Topological Anderson Insulator”. In: *Phys. Rev. Lett.* 103 (2009), p. 196805. DOI: 10.1103/PhysRevLett.103.196805.

[148] D. I. Pikulin, P. G. Silvestrov, and T. Hyart. “Confinement-deconfinement transition due to spontaneous symmetry breaking in quantum Hall bilayers, journal=Nature Communications”. In: 7.1 (2016), p. 10462. DOI: 10.1038/ncomms10462.

[149] L. H. Hu et al. “Effect of in-plane magnetic field and applied strain in quantum spin Hall systems: Application to InAs/GaSb quantum wells”. In: *Phys. Rev. B* 94 (2016), p. 085306. DOI: 10.1103/PhysRevB.94.085306.

[150] L. V. Keldysh and A. N. Kozlov. “Collective properties of excitons in semiconductors”. In: *Journal of Experimental and Theoretical Physics* 27.3 (1968), p. 521.

[151] P. B. Littlewood and X. Zhu. “Possibilities for exciton condensation in semiconductor quantum-well structures”. In: *Physica Scripta* 1996.T68 (1996), p. 56. DOI: 10.1088/0031-8949/1996/T68/008.

[152] Y. E. Lozovik and V.I. Yudson. “Feasibility of superfluidity of paired spatially separated electrons and holes; a new superconductivity mechanism”. In: *Soviet Journal of Experimental and Theoretical Physics Letters* 22 (1975), p. 274.

[153] Y. E. Lozovik and V. I. Yudson. “New mechanism for superconductivity: pairing between spatially separated electrons and holes”. In: *Sov. Phys. JETP* 44.2 (1976), p. 389.

[154] Y. P. Shim and A. H. MacDonald. “Spin-orbit interactions in bilayer exciton-condensate ferromagnets”. In: *Phys. Rev. B* 79 (2009), p. 235329. DOI: 10.1103/PhysRevB.79.235329.

[155] X. Zhu et al. “Exciton Condensate in Semiconductor Quantum Well Structures”. In: *Phys. Rev. Lett.* 74 (1995), pp. 1633–1636. DOI: 10.1103/PhysRevLett.74.1633.

Dostępy do artykułów:

PHYSICAL REVIEW B **106**, 235420 (2022)

Interplay of quantum spin Hall effect and spontaneous time-reversal symmetry breaking in electron-hole bilayers. I. Transport properties

Tania Paul , V. Fernández Becerra, and Timo Hyart

DOI: 10.1103/PhysRevB.106.235420

PHYSICAL REVIEW B 106, 235421 (2022)

Interplay of quantum spin Hall effect and spontaneous time-reversal symmetry breaking in electron-hole bilayers. II. Zero-field topological superconductivity

Tania Paul , V. Fernández Becerra, and Timo Hyart

DOI: 10.1103/PhysRevB.106.235421